Vapor–Liquid Equilibria of Hydrogen Chloride, Phosgene, Benzene, Chlorobenzene, Ortho-Dichlorobenzene, and Toluene by Molecular Simulation

Yow-Lin Huang
Thermodynamics and Energy Technology (ThEt), University of Paderborn, Warburger Str. 100, 33098 Paderborn, Germany

Manfred Heilig
GCP Chemical and Process Engineering, BASF SE, Ludwigshafen, Germany

Hans Hasse
Laboratory of Engineering Thermodynamics (LTD), University of Kaiserslautern, Erwin-Schrödinger-Str. 44, 67663 Kaiserslautern, Germany

Jadran Vrabec
Thermodynamics and Energy Technology (ThEt), University of Paderborn, Warburger Str. 100, 33098 Paderborn, Germany

DOI 10.1002/aic.12329
Published online July 19, 2010 in Wiley Online Library (wileyonlinelibrary.com).

Vapor–liquid equilibria (VLE) of nine binary mixtures containing hydrogen chloride or phosgene in the solvents benzene, chlorobenzene, ortho-dichlorobenzene, and toluene as well as the mixture hydrogen chloride + phosgene are predicted by molecular modeling and simulation. The underlying force fields for the pure substances are developed on the basis of quantum chemical information on molecular geometry and electrostatics. These are individually optimized to experimental pure fluid data on the vapor pressure and saturated liquid density, where the deviations are typically less than 5 and 0.5 %, respectively. The unlike dispersive interaction is optimized for seven of the nine studied binaries. Previously unpublished experimental binary VLE data, measured by BASF in the vicinity of ambient temperature, are predominantly used for these fits. VLE data, including dew point composition, saturated densities and enthalpy of vaporization, are predicted for a wide range of temperatures and compositions. © 2010 American Institute of Chemical Engineers *AIChE J,* 57: 1043–1060, 2011
Keywords: molecular modeling, vapor–liquid equilibrium, critical properties, hydrogen chloride, phosgene, benzene, chlorobenzene, ortho-dichlorobenzene, toluene

Introduction

Molecular modeling and simulation is a modern approach for predicting thermophysical properties of fluids.[1] Based on mathematical representations of the intermolecular

Additional Supporting Information may be found in online version of this article.
Correspondence concerning this article should be addressed to J. Vrabec at jadran.vrabec@upb.de.

interactions, it has strong predictive capabilities as it adequately represents structure, energetics and dynamics on the microscopic scale that govern the fluid behavior on the macroscopic scale.

Backed by the chemical industry, substantial efforts were made in recent years by the molecular simulation community to tackle thermophysical properties of technically relevant fluid systems.[2–6] This is particularly rewarding for substances, which have inconvenient properties like being toxic or explosive, that render experimental studies difficult.

Here, the results from a co-operation between academia and industry, i.e., BASF SE, Ludwigshafen, Germany, are presented. In this work, the fluid phase behavior of hazardous chemicals, which are produced on a large scale, was studied. The investigated molecules are hydrogen chloride, phosgene, benzene, chlorobenzene, ortho-dichlorobenzene, and toluene. For the pure substances, new molecular models were developed in this work on the basis of quantum chemical (QC) calculations and optimizations to the vapor pressure and the saturated liquid density in the first step.

Knowledge on vapor–liquid equilibria (VLE) of binary mixtures of those compounds is crucial for the design and optimization of thermal separation operations, which are part of the respective production processes. However, such data are hardly available from experiment in the public domain.

Hydrogen chloride and phosgene are key components in the production of isocyanates, which are important intermediates in the polyurethane production. The isocyanate synthesis is a phosgenation in which phosgene and hydrogen chloride are present in mixtures with organic solvents, where benzene, chlorobenzene, ortho-dichlorobenzene, and toluene are of special interest. Therefore, in this work, the binary mixtures of hydrogen chloride or phosgene with these four solvents were systematically studied together with the mixture hydrogen chloride + phosgene. This provides a sound basis for modeling the complex multicomponent mixtures of the studied components which are of interest in the production processes.

For binary mixture modeling, an approach was chosen that is similar to the third Industrial Fluid Properties Simulation Challenge.[4] In that competition, experimental data on the bubble line of 1,1,1,2,3,3,3-heptaflouropropane + ethanol were supplied for a low-temperature (283.17 K) over the full composition range. The task was to predict the binary VLE at 343.13 K based on the low-temperature data. The predictions submitted by the participants were then benchmarked to experimental data that were not publicly available before the close of the competition.[4]

For seven binary mixtures studied in this work, i.e., hydrogen chloride + phosgene, hydrogen chloride + benzene, hydrogen chloride + chlorobenzene, hydrogen chloride + toluene, phosgene + chlorobenzene, phosgene + ortho-dichlorobenzne, and phosgene + toluene, BASF supplied a narrow base of predominantly non-public experimental data points on the bubble line. These data, typically a single point per binary system measured around ambient temperature and for compositions that are rich in the high boiling component, were used as a basis to predict the binary VLE at higher temperatures and at other compositions. Subsequent to the computations by molecular simulation, additional, also predominantly non-public experimental VLE data were supplied by BASF to assess the present predictions.

For an eighth mixture, i.e., hydrogen chloride + ortho-dichlorobenzene, a strictly predictive approach was chosen. Binary VLE data for that mixture were generated here on the basis of pure substance properties alone and later on assessed by non-public experimental BASF data.

Finally, for a ninth mixture, i.e., phosgene + benzene, it was tested for one given temperature whether a rather unusual slope of the bubble line can be predicted.

Molecular Model Class

To describe the intermolecular interactions, a varying number of LJ sites and superimposed point charges, point dipoles and linear point quadrupoles were used. Point dipoles and quadrupoles were employed for the description of the electrostatic interactions to reduce the computational effort during simulation. However, a point dipole may, e.g., when a simulation program does not support this interaction site type, be approximated by two point charges $\pm q$ separated by a distance l. Limited to small l, one is free to choose this distance as long as $\mu = ql$ holds. Analogously, a linear point quadrupole can be approximated by three collinear point charges q, $-2q$, and q separated by l each, where $Q = 2ql^2$. The relation between the quadrupole moment Q and the quadrupole tensor was discussed, e.g., in a prior work of our group.[7]

A simulation code that does support point dipole and point quadrupole sites is *ms*2.[8]

The parameters of the present molecular models can be separated into three groups. First, the geometric parameters specify the positions of the different interaction sites of the molecular model. Second, the electrostatic parameters define the polar interactions in terms of point charges, dipoles, and quadrupoles. And finally, the dispersive and repulsive parameters determine the attraction by London forces and the repulsion by overlaps of the electronic orbitals. Here, the Lennard-Jones 12-6 (LJ) potential[9,10] was used to allow for a straightforward compatibility with the overwhelming majority of the molecular models in the literature.

The total intermolecular interaction energy thus writes as

$$
\begin{aligned}
U = \sum_{i=1}^{N-1} \sum_{j=i+1}^{N} \Bigg\{ & \sum_{a=1}^{S_i^{\mathrm{LJ}}} \sum_{b=1}^{S_j^{\mathrm{LJ}}} 4\varepsilon_{ijab} \left[\left(\frac{\sigma_{ijab}}{r_{ijab}} \right)^{12} - \left(\frac{\sigma_{ijab}}{r_{ijab}} \right)^{6} \right] \\
& + \sum_{c=1}^{S_i^{\mathrm{e}}} \sum_{d=1}^{S_j^{\mathrm{e}}} \frac{1}{4\pi\varepsilon_0} \Bigg[\frac{q_{ic} q_{jd}}{r_{ijcd}} + \frac{q_{ic}\mu_{jd} + \mu_{ic} q_{jd}}{r_{ijcd}^2} \cdot f_1(\boldsymbol{\omega}_i, \boldsymbol{\omega}_j) \\
& + \frac{q_{ic} Q_{jd} + Q_{ic} q_{jd}}{r_{ijcd}^3} \cdot f_2(\boldsymbol{\omega}_i, \boldsymbol{\omega}_j) + \frac{\mu_{ic}\mu_{jd}}{r_{ijcd}^3} \cdot f_3(\boldsymbol{\omega}_i, \boldsymbol{\omega}_j) \\
& + \frac{\mu_{ic} Q_{jd} + Q_{ic}\mu_{jd}}{r_{ijcd}^4} \cdot f_4(\boldsymbol{\omega}_i, \boldsymbol{\omega}_j) + \frac{Q_{ic} Q_{jd}}{r_{ijcd}^5} \cdot f_5(\boldsymbol{\omega}_i, \boldsymbol{\omega}_j) \Bigg] \Bigg\},
\end{aligned}
\tag{1}
$$

where r_{ijab}, ε_{ijab}, σ_{ijab} are the distance, the LJ energy parameter, and the LJ size parameter, respectively, for the pair-wise interaction between LJ site a on molecule i and LJ site b on molecule j. The permittivity of vacuum is ε_0, whereas q_{ic}, μ_{ic}, and Q_{ic} denote the point charge magnitude, the dipole

moment, and the quadrupole moment of the electrostatic interaction site c on molecule i and so forth. The expressions $f_x(\omega_i,\omega_j)$ stand for the dependency of the electrostatic interactions on the orientations ω_i and ω_j of the molecules i and j.[11,12] Finally, the summation limits N, S_x^{LJ}, and S_x^e denote the number of molecules, the number of LJ sites, and the number of electrostatic sites, respectively.

For a given molecule, i.e., in a pure fluid throughout, the interactions between LJ sites of different type were defined by applying the standard Lorentz-Berthelot combining rules[13,14]

$$\sigma_{ijab} = \frac{\sigma_{iiaa} + \sigma_{jjbb}}{2}, \tag{2}$$

and

$$\varepsilon_{ijab} = \sqrt{\varepsilon_{iiaa}\varepsilon_{jjbb}}. \tag{3}$$

Molecular Properties from Quantum Chemistry

Molecular models that were developed on the basis of QC calculations stand between ab initio models and empirical models. The present strategy is based on the idea to include ab initio information without giving up the freedom to reasonably optimize the model to important macroscopic thermodynamic properties. Thus, for the modeling process, some experimental data are needed for optimization. The chosen properties, vapor pressure and saturated liquid density, have the advantage to be well available for numerous engineering fluids and to represent dominant features of the fluid state.

In a recent publication, Sandler and Castier[15] gave a brief overview on the use of QC in thermodynamics. By numerically solving Schrödinger's equation, different molecular properties of technically relevant components can be calculated in a quite standardized way. Many different QC codes are available for this task. For license reasons, the open source code GAMESS(US)[16] was used in this work.

Geometry

All geometric data of the molecular models, i.e. bond lengths, angles, and dihedrals, were determined based on QC calculations. Therefore, a geometry optimization, i.e. an energy minimization, was initially performed using GAMESS(US).[16] The Hartree-Fock level of theory was applied with a relatively small (6-31G) basis set.

The resulting configuration of the atoms was taken to specify the spatial distribution of the LJ sites, except for the sites that represent groups containing hydrogen atoms. As the united atom approach was used to obtain computationally efficient molecular models, the dispersive and repulsive interactions of the hydrogen atoms were modeled together with the atom they are bonded to. For the methyl (CH_3) united atom site, the LJ potential was located at the geometric mean of the nuclei, while the methine (CH) united atom site was located at 0.4 of the distance between carbon and hydrogen atom. These empirical offsets are in good agreement with the results of Ungerer et al.,[17] which were found by optimization of transferable molecular models for *n*-alkanes.

Electrostatics

Intermolecular electrostatic interactions mainly occur due to static polarities of single molecules that can well be obtained by QC. Here, the Møller-Plesset 2 level was used that considers electron correlation in combination with the polarizable 6-311G(d,p) basis set.

The purpose of this work was the development of effective pair potentials with state-independent model parameters. Obviously, the electrostatic interactions are stronger in the liquid state than in the gaseous state because of the higher density. Furthermore, the mutual polarization raises their magnitude in the liquid. Thus, for the calculation of the electrostatic moments by QC, a liquid-like state should be considered. This was done here by placing one molecule into a dielectric continuum and assigning the experimental dielectric constant of the liquid to it, as in the COSMO method.

From the resulting electron density distribution for the small symmetric molecules studied here, the dipole and quadrupole moments were estimated by simple integration over the orbitals. Thus, magnitudes and orientations of these electrostatic interaction sites were derived from QC calculations.

Dispersion and repulsion

It would be highly desirable to also calculate the dispersive and repulsive interactions using ab initio methods as well. This approach was followed by different authors in the past, e.g. for neon,[18–21] argon,[19,21,22] krypton,[23] nitrogen,[24] carbon dioxide,[25] hydrogen chloride,[26] acetonitrile,[27] methanol,[27] acetylene,[28] or methanethiol.[29] However, from an engineering point of view, this leads to difficulties.

For an estimation of dispersive and repulsive interactions, at least two molecules must be taken into account. To properly scan the energy hyper surface, many QC calculations at different distances and orientations of the molecules have to be performed. As the dispersive, and partly also the repulsive, interactions are usually only a very small fraction of the total energy calculated by QC, highly accurate methods like coupled cluster (CC) with large basis sets or even extrapolations to the basis set limit must be used for this task.[15]

Because of the fact that this is computationally too expensive for engineering purposes, LJ parameters for a given atom or molecular group were passed on from other molecular models. Some of these parameters were subsequently fitted in the optimization process to yield an accurate VLE behavior of the modeled pure substance.

Pure Fluid Models

None of the six molecules studied in this work exhibit significant conformational changes. Their internal degrees of freedom were thus neglected, and the molecular models were chosen to be rigid, using the most stable configuration as determined by QC.

The optimization was performed using a Newton scheme following Stoll.[30,31] The applied method has many

similarities with the one published by Bourasseau et al.[32] It relies on a least-square minimization of a weighted fitness function that quantifies the deviations of simulation results for a given molecular model compared with reference data.

Correlations for vapor pressure, saturated liquid density, and enthalpy of vaporization, taken from the DIPPR database,[33] were used as reference data for model adjustment and evaluation. This was done even in cases where the correlations are based only on few true experimental data points, as they were regarded as best practice. The quantitative comparison between simulation results and correlations was done by applying fits to the simulation data according to Lotfi et al.[34] The relative deviation between fit and correlation was calculated in steps of 1 K in the temperature range where simulations were performed and is denoted by "mean unsigned error" in the following.

VLE were simulated with the Grand Equilibrium method,[35] the technical details are given in the appendix. The optimized parameter sets of the new molecular models are summarized in Table 1.

The pure substance VLE simulation results on the basis of these optimized models are shown in absolute terms in Figures 1 to 4, where they are compared to the DIPPR correlations. Numerical simulation results for vapor pressure, saturated densities, and enthalpy of vaporization are given in Table 2.

Figure 2 illustrates the influence of molecular size and polarity on the phase envelope in a systematic manner. Both size and polarity increase in the sequence benzene, chlorobenzene, and ortho-dichlorobenzene, which is reflected by a decreasing average saturated liquid density and an increasing critical temperature.

The critical properties were determined through fits to the present VLE simulation results as suggested by Lotfi et al.[34] The estimated uncertainties of critical temperature, critical density, and critical pressure from simulation are 1, 3, and 3 %, respectively. Table 3 compares these critical properties to experimental data.[36–40] An excellent agreement was achieved, being almost throughout within the combined error bars.

For hydrogen chloride, phosgene, and benzene, experimental data on the second virial coefficient are available.[41–44] Figure 5 compares the predictions based on the present molecular models with these data. The agreement is very good, only at low temperatures noticeable deviations are present for the smaller two molecules.

In the following sections, substance specific details are discussed, and the model optimization results are assessed by means of deviation plots. Thereby, models from the literature are compared to the present models as far as available.

Hydrogen chloride

The intermolecular interactions of hydrogen chloride were described by one LJ site plus two point charges, being located exactly at the positions of the hydrogen atom and the chlorine atom as determined by QC. During the optimization of the model parameters to vapor pressure and saturated liquid density, the magnitude of the point charges was altered, only by 3.5% leading to a dipole moment of 5.600×10^{-30} Cm which is thus close to the one determined by QC (5.411×10^{-30} Cm).

The experimental dipole moment of Hydrogen chloride is 3.698×10^{-30} Cm.[45] It can be argued that this elevated polar moment is necessary as the model's point charges have to cover both polarity and hydrogen bonding.[46]

Figure 6 shows deviation plots between simulation and correlations, where also simulation results from Meredith et al.[47] and experimental data[36,48] are included. A very good agreement was obtained for the present model, yielding mean unsigned errors in vapor pressure, saturated liquid density, and enthalpy of vaporization of 2.0, 0.4, and 4.4 %, respectively, in the temperature range from 180 to 310 K, which is about 55 to 96 % of the critical temperature. It should be pointed out that the DIPPR correlations deviate from the actual experimental data roughly to the same extent as the present simulation results. Data by Meredith et al. show a significant scatter, particularly for the saturated liquid density. The deviations are approximately one order of magnitude larger than those of this work. Note that Meredith et al. did not publish data on the enthalpy of vaporization.

Phosgene

The present Phosgene model consists of four LJ sites, i.e. one for every atom, plus one relatively weak dipole (3.341×10^{-30} Cm) and one relatively strong quadrupole (-12.098×10^{-40} Cm^2). Compared to the QC results, the geometry of that molecular model was slightly scaled by 0.2 %, i.e., the bond lengths were increased by that fraction. However, the polar moments had to be reduced more significantly, i.e. by -32 % and -17 % for the dipole and quadrupole moment, respectively, to achieve the optimization result. The experimental dipole moment, being 3.903×10^{-30} Cm,[49] is closer to the molecular model than to the QC result.

Figure 7 presents deviation plots between simulation and correlations, including simulation results from Wu et al.[50] and experimental data.[37,51] Again, a very good agreement was obtained for the present model, yielding mean unsigned errors in vapor pressure, saturated liquid density, and enthalpy of vaporization of 2.1, 0.5, and 3.0 %, respectively, in the temperature range from 230 to 424 K, which is about 50 to 93 % of the critical temperature. There is only a single experimental data point for the saturated liquid density. That is fully in line with the present molecular model. The experimental data for the vapor pressure deviate from the correlation in a sinusoidal fashion with extremal values of around ± 3 %, which indicates questionable fitting by DIPPR. With respect to the enthalpy of vaporization, the present simulation data exhibit an almost constant positive offset. The present model shows more reliable results than the one by Wu et al. for both saturated liquid density and vapor pressure, particularly because of lower statistical noise. No comparison between the models was possible for the enthalpy of vaporization as numerical data were not published by Wu et al.

Benzene

Different molecular models for Benzene can be found in the literature, which are mostly based on six LJ sites plus one quadrupole in the center of the molecule that is oriented perpendicular to the molecular plane. Initially, we have chosen the same model type in this work; however, it was found

Table 1. Parameters of the New Molecular Models

Interaction site	x (Å)	y (Å)	z (Å)	σ (Å)	ε/k_B (Å)	θ (deg)	φ (deg)	$q\ 10^{-19}$ (C)	$\mu\ 10^{-30}$ (Cm)	$Q\ 10^{-40}$ (Cm^2)
Hydrogen chloride										
HCl	0	0	−0.0378	3.520	179.00					
point charge(H)	0	0	1.2422					0.438		
point charge(Cl)	0	0	−0.0378					−0.438		
Phosgene										
C	0	0.5049	0	2.815	10.62					
O	0	1.7018	0	3.195	132.66					
Cl(1)	0	−0.4695	−1.4509	3.366	157.63					
Cl(2)	0	−0.4695	1.4509	3.366	157.63					
Dipole	0	0.0845	0			90	90		3.341	
Quadrupole	0	0	0			90	90			−12.098
Benzene										
CH(1)	0	1.5843	0.9147	3.243	91.82					
CH(2)	0	1.5843	−0.9147	3.243	91.82					
CH(3)	0	0	−1.8294	3.243	91.82					
CH(4)	0	−1.5843	−0.9147	3.243	91.82					
CH(5)	0	−1.5843	0.9147	3.243	91.82					
CH(6)	0	0	1.8294	3.243	91.82					
Quadrupole(1)	0	1.5843	0.9147			90	0			−3.429
Quadrupole(2)	0	1.5843	−0.9147			90	0			−3.429
Quadrupole(3)	0	0	−1.8294			90	0			−3.429
Quadrupole(4)	0	−1.5843	−0.9147			90	0			−3.429
Quadrupole(5)	0	−1.5843	0.9147			90	0			−3.429
Quadrupole(6)	0	0	1.8294			90	0			−3.429
Chlorobenzene										
CH(1)	0	0	2.7329	3.306	96.39					
CH(2)	0	−1.5723	1.8201	3.306	96.39					
CH(3)	0	1.5723	1.8201	3.306	96.39					
CH(4)	0	−1.5761	0.0025	3.306	96.39					
CH(5)	0	1.5761	0.0025	3.306	96.39					
C	0	0	−0.4563	2.787	11.66					
Cl	0	0	−2.1844	3.373	176.30					
Dipole	0	0	−0.4563			0	−90		7.238	
Quadrupole(1)	0	0	2.7329			90	0			−6.055
Quadrupole(2)	0	−1.5723	1.8201			90	0			−6.055
Quadrupole(3)	0	1.5723	1.8201			90	0			−6.055
Quadrupole(4)	0	−1.5761	0.0025			90	0			−6.055
Quadrupole(5)	0	1.5761	0.0025			90	0			−6.055
Ortho-Dichlorobenzene										
C(1)	0	0.6908	0.0051	2.771	11.46					
C(2)	0	−0.6908	0.0051	2.771	11.46					
CH(1)	0	0.9056	2.7612	3.413	102.32					
CH(2)	0	−0.9056	2.7612	3.413	102.32					
CH(3)	0	1.8027	1.1948	3.413	102.32					
CH(4)	0	−1.8027	1.1948	3.413	102.32					
Cl(1)	0	1.5813	−1.4524	3.354	173.25					
Cl(2)	0	−1.5813	−1.4524	3.354	173.25					
Dipole	0	0	0.2400			0	−90		10.840	
Quadrupole(1)	0	0.9056	2.7612			90	0			−7.327
Quadrupole(2)	0	−0.9056	2.7612			90	0			−7.327
Quadrupole(3)	0	1.8027	1.1948			90	0			−7.327
Quadrupole(4)	0	−1.8027	1.1948			90	0			−7.327
Toluene										
CH_3	0	0	−2.7520	3.586	123.49					
C	0	0	−0.9597	2.794	10.94					
CH(1)	0	1.5720	−0.4615	3.276	100.52					
CH(2)	0	−1.5720	−0.4615	3.276	100.52					
CH(3)	0	1.5752	1.3557	3.276	100.52					
CH(4)	0	−1.5752	1.3557	3.276	100.52					
CH(5)	0	0	2.2729	3.276	100.52					
Dipole	0	0	−0.9597			180	−90		1.468	
Quadrupole(1)	0	1.5720	−0.4615			90	0			−5.630
Quadrupole(2)	0	−1.5720	−0.4615			90	0			−5.630
Quadrupole(3)	0	1.5752	1.3557			90	0			−5.630
Quadrupole(4)	0	−1.5752	1.3557			90	0			−5.630
Quadrupole(5)	0	0	2.2729			90	0			−5.630

Lennard-Jones interaction sites are denoted by the modeled atoms. Electrostatic interaction sites are denoted by point charge, dipole, or quadrupole, respectively. Coordinates are given with respect to the center of mass in a principal axes system. Orientations of the electrostatic sites are defined in standard Euler angles, where φ is the azimuthal angle with respect to the $x - z$ plane and θ is the inclination angle with respect to the z axis.

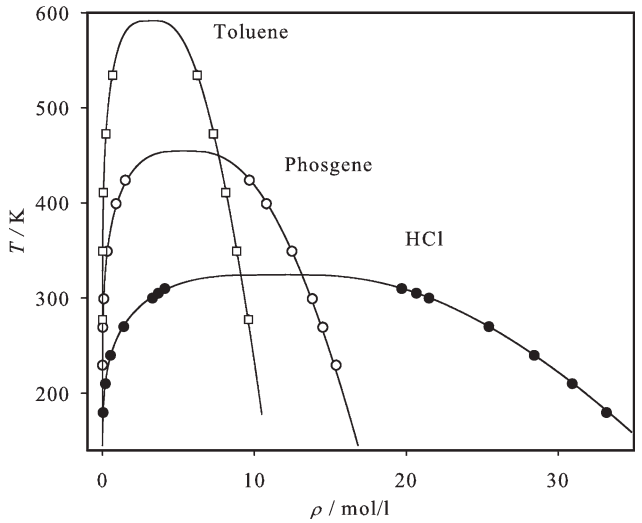

Figure 1. Saturated densities; present simulation data: ● hydrogen chloride, ○ phosgene, □ toluene; correlations of experimental data[33]: —.

to be incompatible with the hydrogen chloride model to describe mixtures with this component. The central quadrupole of the benzene model is hardly shielded by LJ sites so that the hydrogen point charge of hydrogen chloride, which is strongly attracted to it, enters into the central cavity. Eventually, this leads to an extreme pairwise electrostatic energy minimum and to the breakdown of simulation. Therefore, the quadrupole was equally divided into six parts and located on the six LJ sites representing the methine groups, cf. Supporting Information for a graphical schematic. That arrangement is also physically more sound than the initial one. Again, during the optimization process, the geometry was slightly scaled down (−0.1 %), while the total quadrupolar moment was reduced more significantly (−31 %).

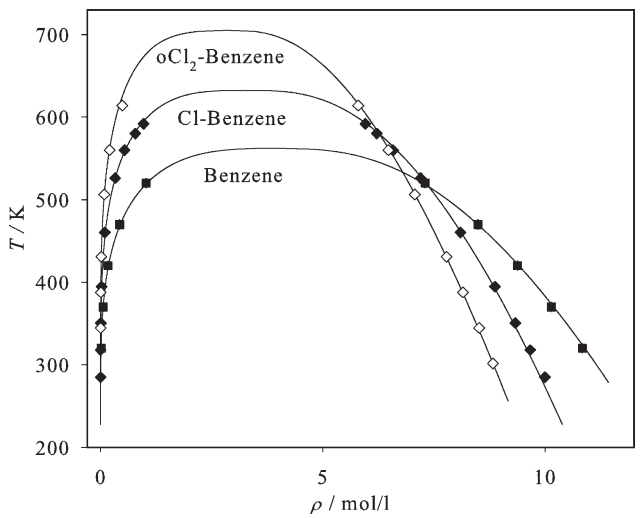

Figure 2. Saturated densities; present simulation data: ■ benzene, ◆ chlorobenzene, ◇ ortho-dichlorobenzene; correlations of experimental data[33]: —.

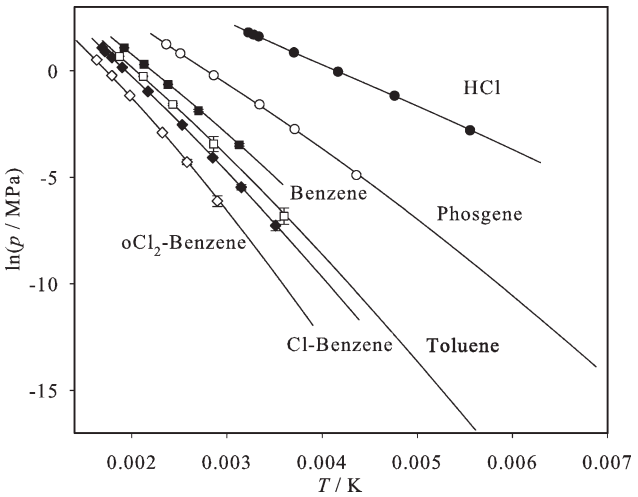

Figure 3. Vapor pressure; present simulation data: ● hydrogen chloride, ○ phosgene, ■ benzene, □ toluene, ◆ chlorobenzene, ◇ ortho-dichlorobenzene; correlations of experimental data[33]: —.

Figure 8 shows the deviation plots, where also simulation results from Bonnaud et al.,[52] Carrero-Mantilla[53], Errington and Panagiotopoulos,[54] Contreras-Camacho et al.,[55] Wick et al.[56] as well as several sets of experimental data[38,57,58] are included. A very good agreement was obtained for the present model, yielding mean unsigned errors in vapor pressure, saturated liquid density, and enthalpy of vaporization of 3.4, 0.4, and 5.2 %, respectively, in the temperature range from 320 to 520 K, which is about 57 to 92 % of the critical temperature.

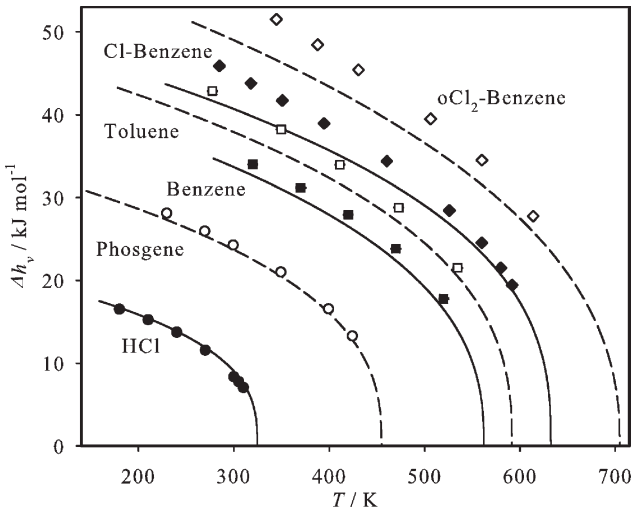

Figure 4. Enthalpy of vaporization; present simulation data: ● hydrogen chloride, ○ phosgene, ■ benzene, □ toluene, ◆ chlorobenzene, ◇ ortho-dichlorobenzene; correlations of experimental data[33]: —, --.

Note that the empty symbols correspond to the dashed lines.

Table 2. Vapor–liquid Equilibrium Simulation Results of the Pure Substances on the Basis of the New Molecular Models

T (K)	p (MPa)	ρ' (mol/l)	ρ'' (mol/l)	Δh_v (kJ/mol)
Hydrogen chloride				
180.00	0.061 (3)	33.19 (1)	0.040 (2)	16.527 (4)
210.00	0.308 (9)	30.92 (1)	0.129 (4)	15.246 (5)
240.00	0.95 (1)	28.42 (2)	0.530 (6)	13.743 (6)
270.00	2.37 (2)	25.45 (3)	1.39 (1)	11.586 (9)
300.00	4.99 (3)	21.50 (2)	3.30 (2)	8.38 (2)
305.00	5.47 (3)	20.66 (3)	3.67 (2)	7.78 (2)
310.00	5.98 (4)	19.70 (3)	4.10 (3)	7.08 (3)
Phosgene				
229.52	0.0081 (3)	15.390 (5)	0.0020 (1)	28.12 (1)
269.43	0.065 (3)	14.499 (6)	0.030 (1)	25.95 (1)
299.37	0.200 (8)	13.819 (6)	0.086 (3)	24.26 (1)
349.27	0.80 (1)	12.480 (8)	0.314 (4)	21.02 (1)
399.16	2.25 (2)	10.80 (2)	0.901 (8)	16.55 (3)
424.11	3.48 (2)	9.66 (2)	1.500 (9)	12.31 (5)
Benzene				
320.00	0.0310 (1)	10.833 (2)	0.00950 (3)	34.00 (1)
370.00	0.154 (3)	10.140 (3)	0.052 (1)	31.18 (1)
395.00	0.313 (1)	9.815 (2)	0.102 (9)	28.23 (8)
420.00	0.524 (8)	9.378 (4)	0.166 (3)	27.93 (2)
445.00	0.885 (4)	8.970 (6)	0.283 (4)	24.57 (8)
470.00	1.348 (9)	8.491 (6)	0.426 (3)	23.81 (2)
520.00	2.92 (2)	7.30 (2)	1.023 (7)	17.79 (6)
Chlorobenzene				
284.96	0.0007 (1)	9.994 (4)	0.00020 (3)	45.87 (2)
317.84	0.0042 (4)	9.664 (4)	0.0010 (1)	43.79 (3)
350.72	0.017 (1)	9.327 (4)	0.0050 (3)	41.71 (2)
394.56	0.079 (3)	8.870 (4)	0.0210 (7)	38.96 (2)
460.32	0.38 (2)	8.093 (7)	0.095 (5)	34.39 (3)
526.08	1.17 (2)	7.20 (3)	0.327 (6)	28.43 (5)
560.00	1.87 (2)	6.58 (1)	0.536 (6)	24.53 (7)
580.00	2.45 (2)	6.21 (2)	0.779 (6)	21.51 (9)
591.84	2.95 (2)	5.96 (1)	0.967 (7)	19.4 (2)
Ortho-Dichlorobenzene				
344.64	0.0022 (2)	8.515 (3)	0.00050 (5)	51.51 (3)
387.72	0.0138 (5)	8.150 (4)	0.0040 (1)	48.44 (3)
430.80	0.055 (2)	7.781 (4)	0.0140 (5)	45.41 (3)
506.19	0.311 (6)	7.066 (7)	0.080 (2)	39.51 (4)
560.04	0.800 (9)	6.48 (2)	0.202 (2)	34.51 (6)
613.89	1.66 (2)	5.79 (2)	0.489 (6)	27.75 (7)
Toluene				
277.51	0.00109 (4)	9.614 (4)	0.00040 (1)	42.85 (3)
349.45	0.03200 (5)	8.837 (2)	0.00160 (1)	38.23 (1)
411.12	0.2050 (5)	8.123 (2)	0.0604 (1)	33.95 (1)
472.79	0.766 (5)	7.311 (5)	0.229 (1)	28.78 (2)
534.46	1.96 (1)	6.23 (1)	0.659 (3)	21.52 (3)

The number in parentheses indicates the statistical uncertainty in the last digit.

Among the six molecular models, the one by Bonnaud et al. has the best performance for both saturated liquid density (mean unsigned error lower than 0.1 %) and enthalpy of vaporization (lower than 2 %); however, it performs poorly for the vapor pressure (about 18 %). Similarly, saturated density and enthalpy of vaporization are quite well represented by the model of Contreras-Camacho, but more significant deviations are present for the vapor pressure. The model of Errington and Panagiotopoulos performs well for both saturated liquid density (about 0.4 %) and vapor pressure (about 3 %), but its description of the enthalpy of vaporization is very poor. The model of Carrero-Mantilla describes the vapor pressure well (about 5 %), but large deviations are present for the remaining two properties. Finally, the model

Table 3. Critical Properties of the Pure Substances on the Basis of the New Molecular Models in Comparison to Recommended Experimental Data

	T_c^{sim} (K)	T_c^{exp} (K)	ρ_c^{sim} (mol/l)	ρ_c^{exp} (mol/l)	p_c^{sim} (MPa)	p_c^{exp} (MPa)	Ref.
Hydrogen chloride	324	324.65 (5)	12.2	12.34 (3)	8.3	8.31 (5)	36
Phosgene	454	455.0 (7)	5.1	5.40 (6)	5.7	5.35 (4)	37
Benzene	563	562.15 (6)	3.9	3.88 (2)	4.9	4.9 (1)	38
Chlorobenzene	631	632.35 (8)	3.2	3.24 (7)	4.6	4.52 (8)	39
Ortho-Dichlorobenzene	705	705.0 (9)	2.8	2.77 (6)	4.0	4.1 (3)	40
Toluene	592	591.75 (8)	3.4	3.20 (4)	4.1	4.08 (3)	38

The number in parentheses indicates the experimental uncertainty in the last digit.

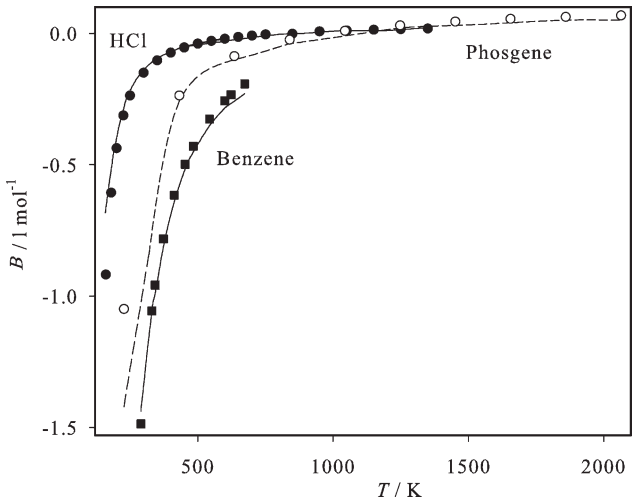

Figure 5. Second virial coefficient; present simulation data: ● hydrogen chloride, ○ phosgene, ■ benzene; correlations of experimental data[41–44]: —, --.

by Wick et al. shows an offset of about 9 % in vapor pressure and enthalpy of vaporization, whereas for the saturated liquid density a different temperature trend is present, where the two points at 500 and 525 K deviate by more than

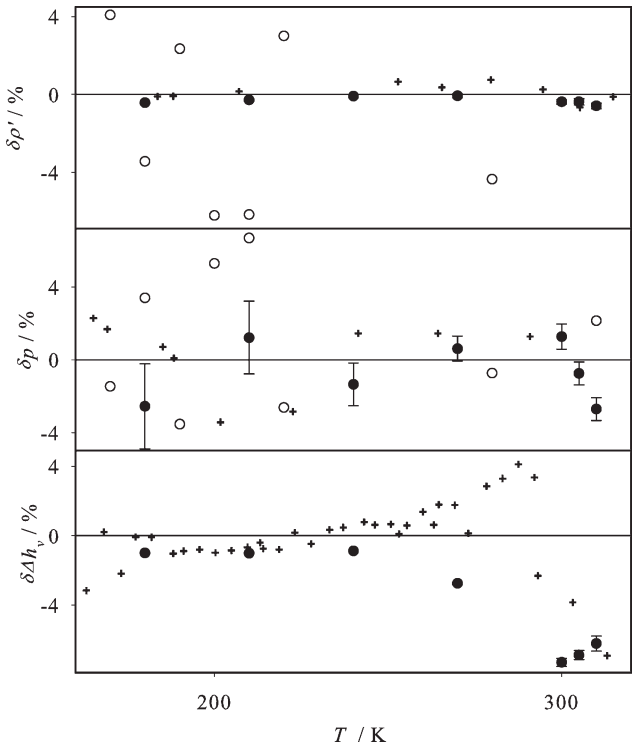

Figure 6. Relative deviations of vapor–liquid equilibrium properties from correlations of experimental data[33] ($\delta z = (z_i - z_{cor})/z_{cor}$) for hydrogen chloride: ● present simulation data, ○ Meredith et al.,[47] + experimental data.[36,48]

Top: saturated liquid density, center: vapor pressure, bottom: enthalpy of vaporization.

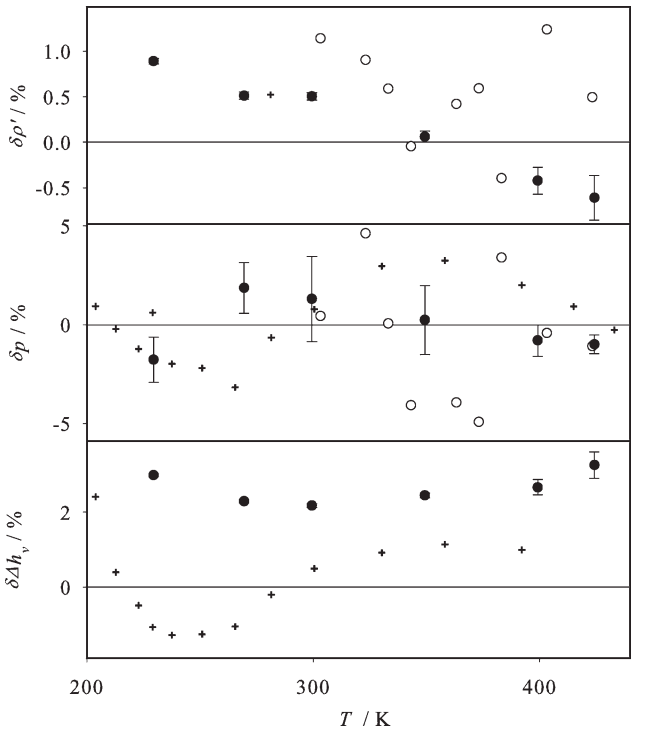

Figure 7. Relative deviations of vapor–liquid equilibrium properties from correlations of experimental data[33] ($\delta z = (z_i - z_{cor})/z_{cor}$) for phosgene: ● present simulation data, ○ Wu et al.,[50] + experimental data.[37,51]

Top: saturated liquid density, center: vapor pressure, bottom: enthalpy of vaporization.

1.5 %. Note that in the deviation plot 8 a substantial number of VLE simulation data points by the other authors is out of scale.

The present modeling approach was independent on the work by Contreras-Camacho et al.,[55] nonetheless the resulting model parameters for geometry and LJ sites are very similar. The difference is less than 0.02 Å for the site positions and the LJ size parameter σ as well as less than 2 % for the LJ energy parameter ε. The difference between the two models thus mainly lies in the different treatment of the electrostatics, which was not explicitly modeled by Contreras-Camacho et al.

Chlorobenzene

For chlorobenzene, seven LJ sites plus one dipole in the molecular plane and five quadrupoles perpendicular to it were chosen. Because of the high electronegativity of the chlorine atom, the dipole moment is quite strong (7.238×10^{-30} Cm), whereas the total quadrupole moment amounts to -30.27×10^{-40} Cm^2. The quadrupole was again equally distributed onto the methine groups to allow for a compatibility with hydrogen chloride in the mixture. Compared to the QC results, the geometry was scaled down by −0.8 %, whereas the polar moments were increased by 3.4 % (dipole) and 6.5 % (quadrupole), respectively. In this case, the experimental dipole moment is 5.944×10^{-30} Cm.[59]

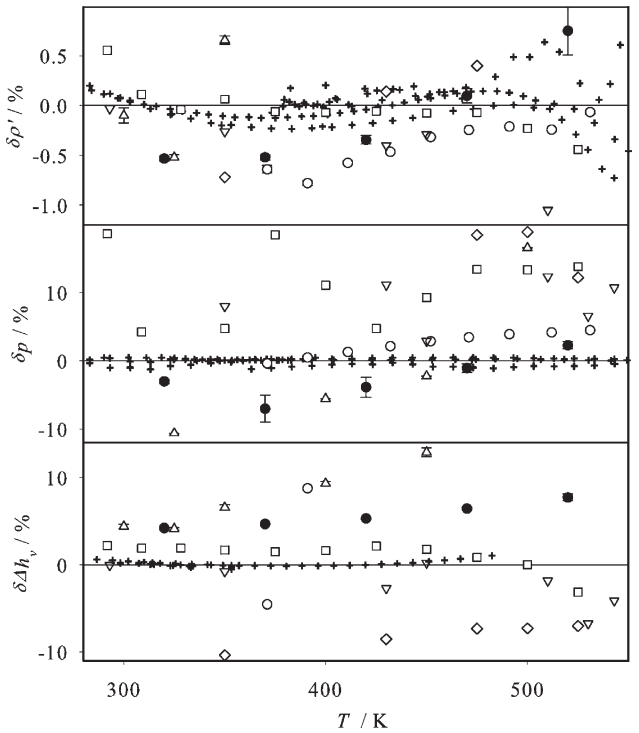

Figure 8. Relative deviations of vapor–liquid equilibrium properties from correlations of experimental data[33] ($\delta z = (z_i - z_{cor})/z_{cor}$) for benzene: ● present simulation data, □ Bonnaud et al.,[52] △ Carrero-Mantilla,[53] ○ Errington and Panagiotopoulos,[54] ▽ Contreras-Camacho et al.,[55] ◇ Wick et al.,[56] + experimental data.[38,57,58]

Top: saturated liquid density, center: vapor pressure, bottom: enthalpy of vaporization.

Figure 9 shows the deviation plots between simulation and correlations including experimental data.[39,60,61] A good agreement was obtained, yielding mean unsigned errors in vapor pressure, saturated liquid density, and enthalpy of vaporization of 5.0, 0.9, and 7.9 %, respectively, in the temperature range from 285 to 592 K, which is about 45 to 94 % of the critical temperature. Although the vapor pressure agrees with the experiment almost throughout within its statistical uncertainty, particularly the enthalpy of vaporization shows a significant positive offset.

No VLE data based on molecular models were found in the literature for this substance.

Ortho-Dichlorobenzene

Eight LJ sites plus four quadrupoles and one strong dipole (10.84×10^{-30} Cm) were used to describe the intermolecular interactions of ortho-dichlorobenzene. The total quadrupole moment of -29.31×10^{-40} Cm^2 was equally distributed onto the four methine groups because of the reasons mentioned above. Compared to the QC results, geometry, dipole, and quadrupole moments of the present ortho-dichlorobenzene model were slightly scaled by −1.4, 1.6, and 0.2 %, respectively. The experimental dipole moment of 8.372×10^{-30} Cm[62] compares well with the model value.

Figure 10 shows the deviation plots between simulation and correlations, where two sets of experimental data[40,63] are included. A good agreement was obtained, yielding mean unsigned errors in vapor pressure, saturated liquid density, and enthalpy of vaporization of 6.4, 0.5, and 9.5 %, respectively, in the temperature range from 345 to 614 K, which is about 50 to 87 % of the critical temperature. Both for vapor pressure and saturated liquid density, the simulation data agree well with the experiment in the range where measurements were made. However, for the enthalpy of vaporization, a significant and almost constant offset is present.

No VLE data based on molecular models were found in the literature for this substance.

Toluene

The present toluene model is composed of seven LJ sites plus five quadrupoles and one weak dipole (1.468×10^{-30} Cm). In contrast to chlorobenzene and ortho-dichlorobenzene, the dipole is oriented from the methyl group toward the center of the molecule. Compared to the QC results, geometry, dipole, and quadrupole moments were marginally scaled by −0.6, 0.5, and 0.3 %, respectively. The experimental dipole moment is 1.251×10^{-30} Cm.[64]

Figure 11 shows deviation plots between simulation and correlations. The deviation plots include simulation results from Nieto-Draghi et al.[65] and Contreras-Camacho et al.[66] as

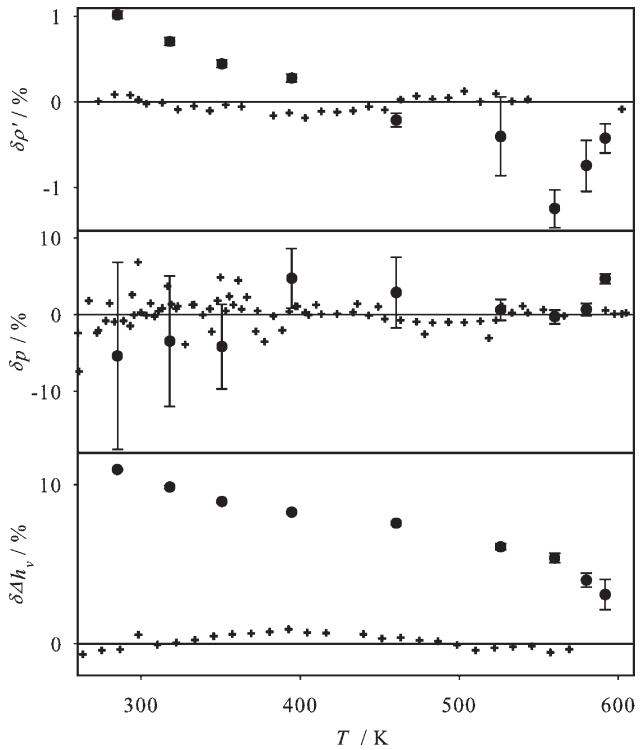

Figure 9. Relative deviations of vapor–liquid equilibrium properties from correlations of experimental data[33] ($\delta z = (z_i - z_{cor})/z_{cor}$) for chlorobenzene: ● present simulation data, + experimental data.[39,60,61]

Top: saturated liquid density, center: vapor pressure, bottom: enthalpy of vaporization.

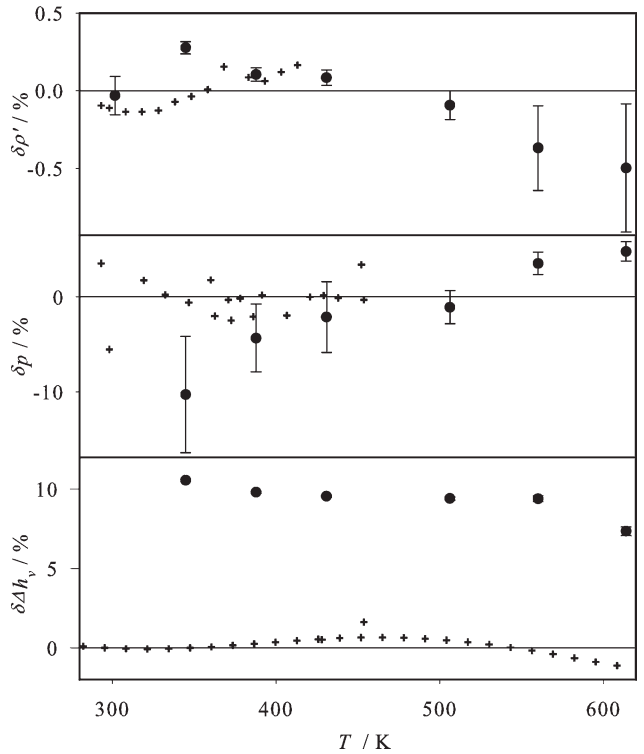

Figure 10. Relative deviations of vapor–liquid equilibrium properties from correlations of experimental data[33] ($\delta z = (z_i - z_{cor})/z_{cor}$) for ortho-dichlorobenzene: ● present simulation data, + experimental data.[40,63]

Top: saturated liquid density, center: vapor pressure, bottom: enthalpy of vaporization.

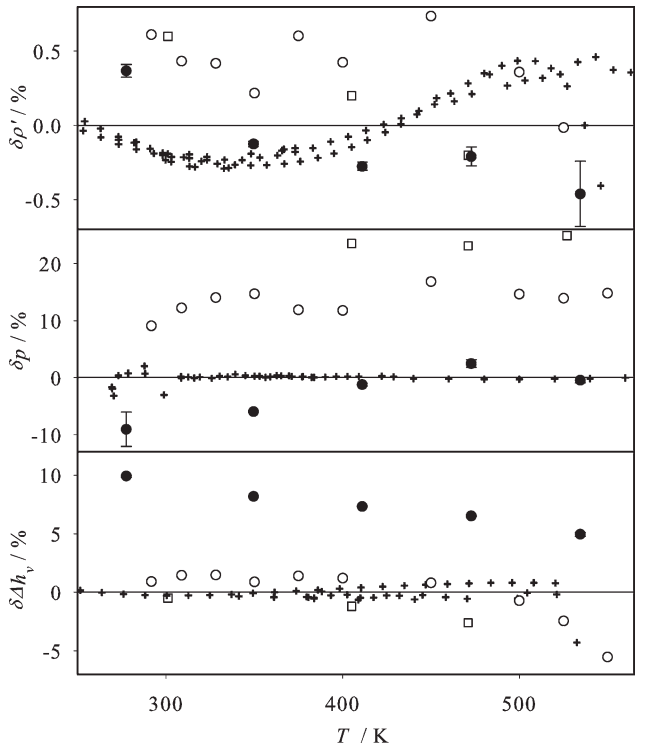

Figure 11. Relative deviations of vapor–liquid equilibrium properties from correlations of experimental data[33] ($\delta z = (z_i - z_{cor})/z_{cor}$) for toluene: ● present simulation data, ○ Nieto-Draghi et al.,[65] □ Contreras-Camacho et al.,[66] + experimental data.[38,57]

Top: saturated liquid density, center: vapor pressure, bottom: enthalpy of vaporization.

well as two sets of experimental data.[38,57] A good agreement was obtained for the present model, yielding mean unsigned errors in vapor pressure, saturated liquid density, and enthalpy of vaporization of 3.9, 0.3, and 7.3 %, respectively, in the temperature range from 278 to 534 K, which is about 47 to 90 % of the critical temperature. The present model leads to more accurate results than the model by Nieto-Draghi et al. for both saturated liquid density and vapor pressure. Nevertheless, the model from Nieto-Draghi et al. shows a much better performance for the enthalpy of vaporization. The model of Contreras-Camacho et al. is of comparable quality, saturated liquid density and enthalpy of vaporization are well represented, whereas significant deviations are present for the vapor pressure.

The geometry of the present toluene model is very similar to the one by Contreras-Camacho et al.[66] (the difference is less than 0.02 Å), which can well be understood as both are based on QC results. Note that the model by Contreras-Camacho et al. does not consider the electrostatic interactions explicitly.

Table 4. Binary Interaction Parameter ξ, Experimental Bubble Point Used for the Adjustment with Reference, Simulation Results with Adjusted ξ and Binary Parameter k_{ij} of the Peng-Robinson EOS

Mixture (A + B)	ξ	T (K)	x_A (mol/mol)	p^{exp} (MPa)	p^{sim} (MPa)	y_A^{sim} (mol/mol)	k_{ij}
Hydrogen chloride + Phosgene	0.751	266.15	0.39	0.84[70]	0.84 (9)	0.95 (1)	0.020
Hydrogen chloride + Benzene	1.112	293.15	0.043	0.101 †	0.104 (2)	0.93 (1)	−0.077
Hydrogen chloride + Chlorobenzene	1.020	283.15	0.094	0.267 †	0.266 (9)	1.000 (0)	0.000
Hydrogen chloride + Ortho-Dichlorobenzene	1.000	393.15	0.133		1.84 (2)	0.9920 (8)	0.000
Hydrogen chloride + Toluene	0.981	293.15	0.048	0.101 †	0.103 (2)	0.983 (4)	−0.075
Phosgene + Benzene	0.960	293.15	0.370	0.086[71]	0.085 (3)	0.935 (7)	0.050
Phosgene + Chlorobenzene	0.990	323.15	0.142	0.065 †	0.067 (3)	0.94 (1)	0.006
Phosgene + Ortho-Dichlorobenzene	1.000	363.15	0.080	0.103 †	0.105 (5)	0.97 (1)	0.020
Phosgene + Toluene	0.990	308.15	0.242	0.072 †	0.069 (3)	0.952 (5)	0.010

The number in parentheses indicates the statistical uncertainty in the last digit. The experimental data from this work is marked by †.

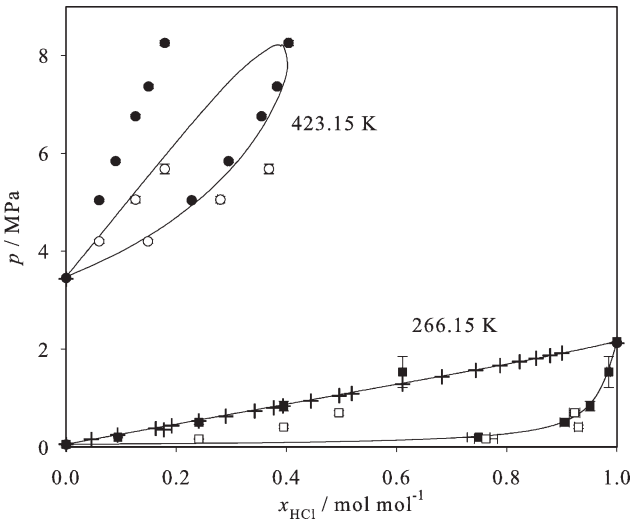

Figure 12. Vapor–liquid phase diagram of hydrogen chloride + phosgene at 266.15 and 423.15 K: + experimental data;[70] ■, ● present simulation data with ξ = 0.751; □, ○ present simulation data with ξ = 1; — Peng-Robinson EOS with k_{ij} = 0.02.

Molecular Mixture Models

On the basis of defined pairwise additive pure fluid models, molecular modeling of mixtures reduces to modeling the interactions between unlike molecules. Unlike interactions consist of two different types here. The unlike electrostatic interactions, e.g. between charge and dipole or dipole and quadrupole and so forth, were treated in a physically straightforward way, simply using the laws of electrostatics.

Unfortunately, the unlike dispersive attraction is not straightforward. If a mixture A + B is modeled on the basis of Lennard-Jones potentials, the knowledge of the unlike LJ parameters σ_{AB} and ε_{AB} is required. Because of the fact that there is no sound physical framework for their determination, the broadly used Lorentz-Berthelot combining rule is the usual starting point[67] with

$$\sigma_{AB} = (\sigma_A + \sigma_B)/2, \tag{4}$$

and

$$\varepsilon_{AB} = \sqrt{\varepsilon_A \varepsilon_B}. \tag{5}$$

Applying σ_{AB} and ε_{AB} as given by Eqs 4 and 5 allows the prediction of mixture properties from pure fluid data alone.[7,30,67–69] But as shown there, a significant improvement can be achieved by introducing one state independent binary parameter ξ to adjust the unlike energy parameters

$$\varepsilon_{AB} = \xi\sqrt{\varepsilon_A \varepsilon_B}. \tag{6}$$

It should be pointed out that A and B are molecule species that may each be described by several LJ sites with different energy parameters ε. Thus, ξ is a single overall parameter that acts consistently on all individual unlike LJ interactions of the pair A + B.

For VLE, it was shown that ξ can be adjusted to a single experimental binary vapor pressure.[67] Specifying temperature and bubble point composition, ξ has hardly any influence on the bubble density and a minor influence on the dew point composition. The benefit of ξ lies in an enhanced representation of the two-phase envelope. The binary parameter was adjusted here following the same procedure.[7,30,69]

Table 4 gives the state point (i.e. temperature T and bubble point mole fraction of the lower boiling component x_A) and the experimental vapor pressure p^{exp} which was used for the adjustment as well as the resulting binary parameter ξ. A first validating VLE simulation at this state point with the adjusted mixture model was performed. The resulting vapor pressure p and dew point composition y_A from simulation are also listed in Table 4 and can numerically be compared to experimental vapor pressure data there.

Binary VLE

Based on the six pure substance models developed in this work, the VLE of nine zeotropic binary mixtures were simulated. These are hydrogen chloride + (benzene, chlorobenzene, ortho-dichlorobenzene and toluene), phosgene with the same four solvents as well as hydrogen chloride + phosgene.

The results are presented here in pressure vs. mole fraction phase diagrams, cf. Figures 12 to 20, where the pure substance vapor pressure of the molecular models is indicated as well. Full numerical VLE simulation data are given in Table 5, which also contains the saturated densities and the heat of vaporization from simulation. Because such data from experiment are not available for comparison, they are not discussed here.

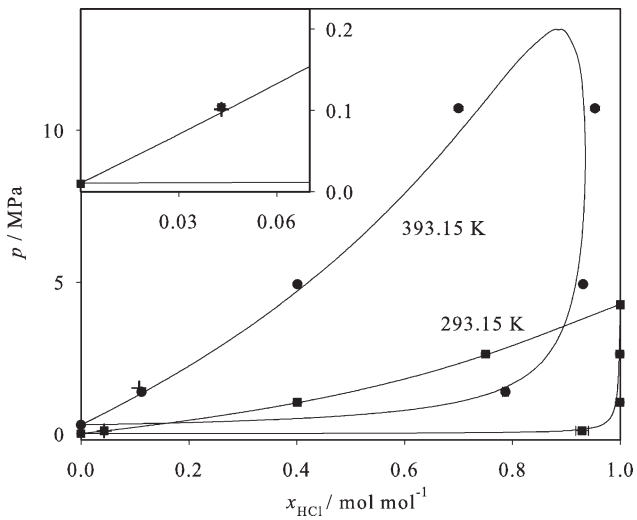

Figure 13. Vapor–liquid phase diagram of hydrogen chloride + benzene at 293.15 and 393.15 K: + experimental data, this work; ■, ● present simulation data with ξ = 1.112; — Peng-Robinson EOS with k_{ij} = −0.077.

Inset: magnified view at the benzene-rich region at 293.15 K.

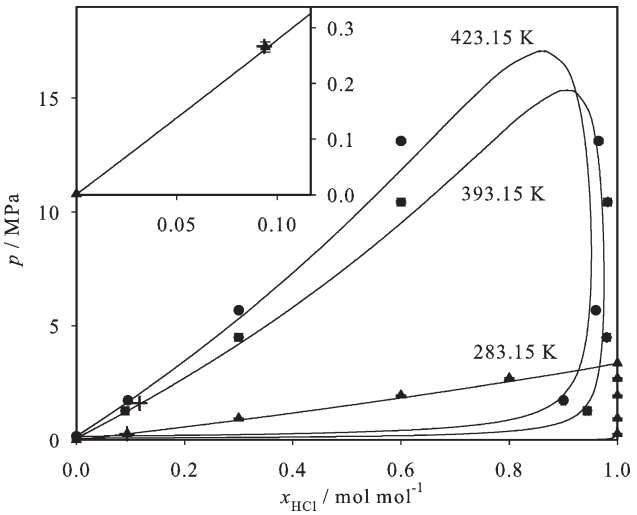

Figure 14. Vapor–liquid phase diagram of hydrogen chloride + chlorobenzene at 283.15, 393.15, and 423.15 K: + experimental data, this work; ▲, ■, ● present simulation data with ξ = 1.020; — Peng-Robinson EOS with k_{ij} = 0.

Inset: magnified view at the chlorobenzene-rich region at 283.15 K.

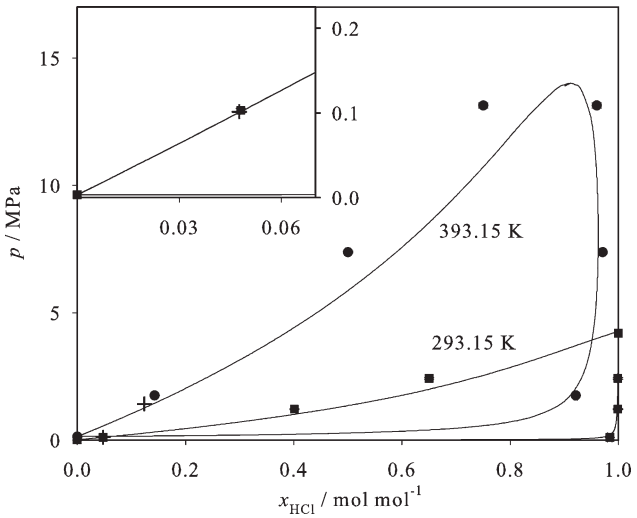

Figure 16. Vapor–liquid phase diagram of hydrogen chloride + toluene at 293.15 and 393.15 K: + experimental data, this work; ■, ● present simulation data with ξ = 0.981; —Peng-Robinson EOS with k_{ij} = −0.075.

Inset: magnified view at the toluene-rich region at 293.15 K.

For all studied mixtures, experimental bubble point data are available for adjustment or comparison. Only for the mixture hydrogen chloride + phosgene, VLE data were measured in the full composition range, whereas for the remaining mixtures, experimental data are available only for compositions which are rich of the high boiling substance. To our knowledge, experimental dew point data were not published at all for any of the studied mixtures.

The experimental approach followed at BASF in this project was: In the pressure range below 0.5 MPa hydrogene chloride or phosgene was transfered into the solvent, and the mass was determined volumetrically or by weighing. The composition of the liquid mixture was corrected by the calculated amounts of the components in the vapor phase. In the pressure range above 0.5 MPa, hydrogene chloride was filled into a visual cell, and the mass was also determined volumetrically or by weighing. The amount of solvent, added

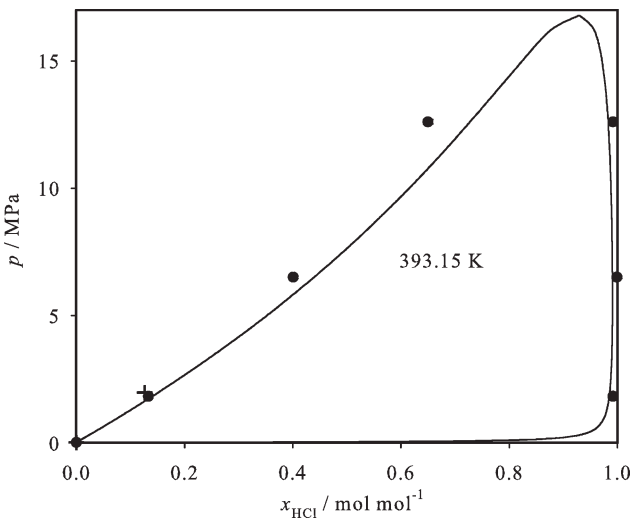

Figure 15. Vapor–liquid phase diagram of hydrogen chloride + ortho-dichlorobenzene at 393.15 K: + experimental data, this work; ● present simulation data with ξ = 1; — Peng-Robinson EOS with k_{ij} = 0.

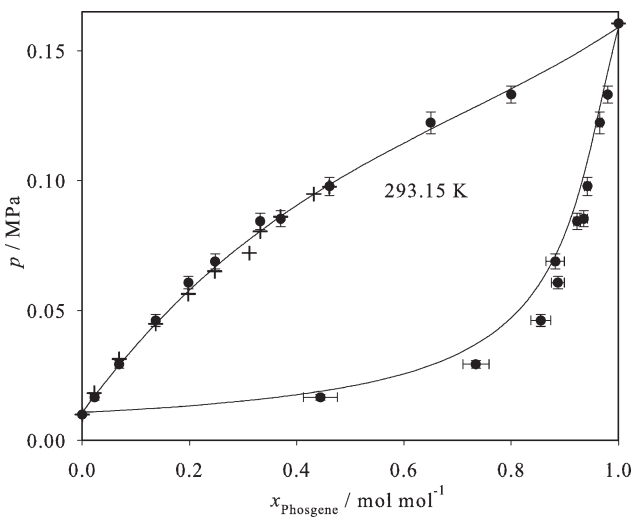

Figure 17. Vapor–liquid phase diagram of phosgene + benzene at 293.15 K: + experimental data;[71] ● present simulation data with ξ = 0.960; — Peng-Robinson EOS with k_{ij} = 0.05.

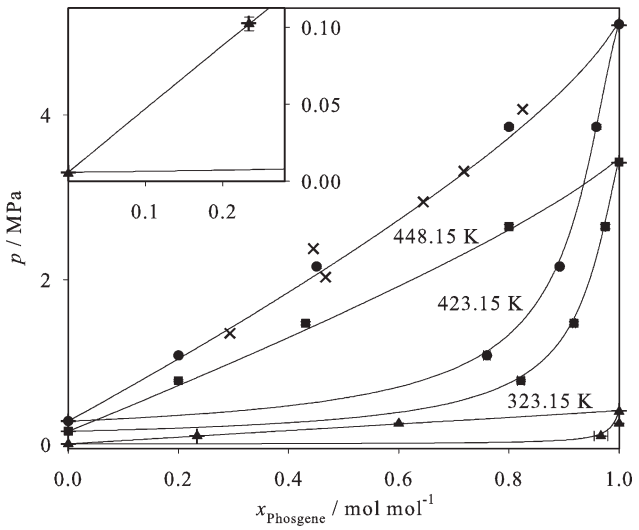

Figure 18. Vapor–liquid phase diagram of phosgene + chlorobenzene at 323.15, 423.15 and 448.15 K: + experimental data, this work; × experimental data;[73] ▲, ■, ● present simulation data with ξ = 0.990; —Peng-Robinson EOS with k_{ij} = 0.006.

Inset: magnified view at the chlorobenzene-rich region at 323.15 K.

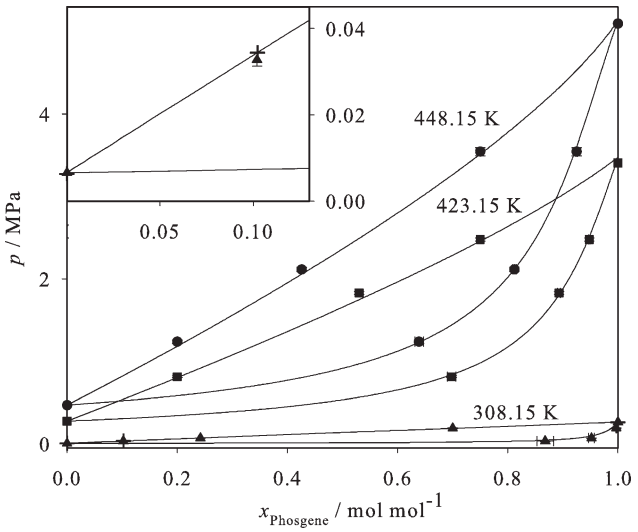

Figure 20. Vapor–liquid phase diagram of phosgene + toluene at 308.15, 423.15, and 448.15 K: + experimental data, this work; ▲, ■, ● present simulation data with ξ = 0.990; — Peng-Robinson EOS with k_{ij} = 0.01.

Inset: magnified view at the toluene-rich region at 308.15 K.

into the cell in order to measure a bubble point, was calculated form the volume displacement in a calibrated spindle press. The experimental uncertainty of the equilibrium data is estimated to be 0.1 K and 2 % relative error in composition and vapor pressure.

For orientation and comparison, the results of the Peng-Robinson equation of state (EOS)[72] with adjusted binary parameter k_{ij} are also shown. The EOS was optimized to the same state point as the molecular model.

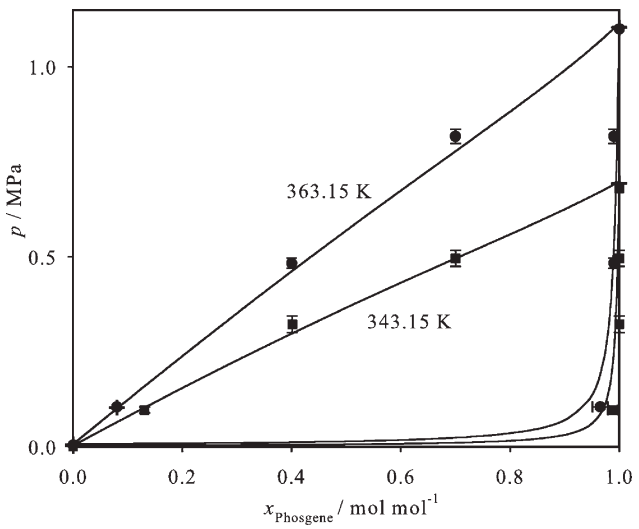

Figure 19. Vapor–liquid phase diagram of phosgene + ortho-dichlorobenzene at 343.15 and 363.15 K: + experimental data, this work; ■, ● present simulation data with ξ = 1; — Peng-Robinson EOS with k_{ij} = 0.02.

Hydrogen chloride + phosgene

Figure 12 shows the VLE of hydrogen chloride + phosgene at 266.15 and 423.15 K from experiment, simulation and Peng-Robinson EOS. At 266.15 K, the mixture is subcritical, the phase envelope is wide with a straight bubble line and a concave dew line. Hydrogen chloride is supercritical at 423.15 K. No experimental data are available so that the simulation data can only be compared to the Peng-Robinson EOS.

The binary parameters $\xi = 0.751$ and $k_{ij} = 0.02$ were adjusted to the vapor pressure measured by Gillespie et al.[70] at 266.15 K for a liquid mole fraction $x_{HCl} = 0.39$ mol/mol. In the phosgene-rich region at 266.15 K, the simulation results agree well with both the experimental data and the Peng-Robinson EOS. However, with increasing mole fraction of hydrogen chloride, the statistical uncertainty strongly increases so that predictions from simulation in the hydrogen chloride-rich region were technically not feasible.

It can be seen in Figure 12 that the predictions at 423.15 K obtained by molecular simulation and those from the Peng-Robinson EOS do not agree, although for the binary parameter adjustment in both cases the same low temperature data point was used. As there are no high temperature experimental data for this system, no ranking of the methods is possible. For comparison, also a prediction by molecular simulation with $\xi = 1$ is included in Figure 12, which is assumed to be less reliable than that with the adjusted ξ. For $\xi = 1$ the results obtained with molecular simulation are close to those from the Peng-Robinson EOS on the bubble line but not on the dew line. Note also that

Table 5. Vapor–Liquid Equilibrium Simulation Results of the Binary Mixtures on the Basis of the New Molecular Models in Partial Comparison to Experimental Vapor Pressure Data

Mixture (A + B)	T (K)	x_A (mol/mol)	p (MPa)	p^{exp} (MPa)	y_A (mol/mol)	ρ' (mol/l)	ρ'' (mol/l)	Δh_v (kJ/mol)
Hydrogen chloride + Phosgene								
	266.15	0.09	0.20 (1)	0.24[70]	0.75 (2)	15.435 (7)	0.092 (5)	25.72 (2)
	266.15	0.24	0.50 (4)	0.53[70]	0.91 (1)	16.861 (7)	0.24 (2)	25.14 (2)
	266.15	0.39	0.84 (9)	0.84[70]	0.95 (1)	18.55 (2)	0.42 (4)	24.07 (3)
	266.15	0.61	1.5 (3)	1.3[70]	0.985 (3)	20.84 (2)	0.82 (16)	20.25 (2)
	423.15	0.06	5.04 (3)		0.228 (1)	9.74 (3)	2.15 (1)	12.26 (5)
	423.15	0.09	5.83 (3)		0.295 (2)	9.78 (2)	2.52 (1)	11.58 (5)
	423.15	0.13	6.75 (4)		0.353 (3)	9.77 (2)	2.98 (2)	10.68 (6)
	423.15	0.15	7.36 (4)		0.383 (3)	9.72 (3)	3.32 (2)	9.95 (8)
	423.15	0.18	8.25 (6)		0.404 (4)	9.78 (4)	3.95 (3)	8.9 (1)
Hydrogen chloride + Benzene								
	293.15	0.043	0.104 (2)	0.101 †	0.93 (1)	11.493 (5)	0.043 (1)	34.50 (2)
	293.15	0.401	1.04 (1)		0.999 (1)	14.770 (9)	0.460 (4)	26.76 (2)
	293.15	0.750	2.63 (3)		0.999 (1)	20.05 (2)	1.33 (2)	18.06 (2)
	393.15	0.108		1.51 †				
	393.15	0.112	1.39 (1)		0.787 (5)	10.463 (7)	0.453 (2)	27.56 (2)
	393.15	0.401	4.93 (2)		0.931 (2)	12.50 (1)	1.786 (7)	20.80 (3)
	393.15	0.700	10.72 (6)		0.953 (1)	14.97 (4)	4.95 (3)	11.95 (6)
Hydrogen chloride + Chlorobenzene								
	283.15	0.094	0.266 (9)	0.267 †	0.997 (3)	10.657 (5)	0.115 (4)	42.83 (3)
	283.15	0.300	0.95 (2)		0.998 (2)	12.471 (5)	0.434 (9)	35.86 (2)
	283.15	0.600	1.98 (3)		0.998 (2)	16.393 (2)	1.00 (2)	25.48 (2)
	283.15	0.800	2.65 (3)		0.999 (1)	20.37 (1)	1.45 (2)	18.32 (2)
	393.15	0.090	1.259 (8)		0.945 (3)	9.395 (5)	0.400 (3)	36.26 (2)
	393.15	0.117		1.61 †				
	393.15	0.300	4.43 (3)		0.980 (1)	10.850 (8)	1.53 (1)	29.10 (3)
	393.15	0.600	10.31 (5)		0.982 (1)	13.61 (1)	4.44 (2)	17.88 (4)
	423.15	0.095	1.73 (1)		0.902 (4)	9.053 (8)	0.577 (3)	34.25 (3)
	423.15	0.300	5.69 (2)		0.959 (1)	10.380 (3)	1.853 (7)	27.25 (2)
	423.15	0.600	12.90 (6)		0.964 (1)	12.74 (3)	5.12 (2)	15.90 (7)
Hydrogen chloride + Ortho-Dichlorobenzene								
	393.15	0.127		1.97 †				
	393.15	0.133	1.84 (2)		0.9920 (8)	8.897 (4)	0.588 (6)	42.74 (3)
	393.15	0.401	6.50 (5)		0.9990 (9)	11.008 (7)	2.36 (2)	31.24 (3)
	393.15	0.651	12.60 (8)		0.9921 (6)	13.84 (2)	5.79 (4)	19.06 (5)
Hydrogen chloride + Toluene								
	293.15	0.048	0.103 (2)	0.101 †	0.983 (4)	9.753 (3)	0.043 (1)	40.60 (2)
	293.15	0.401	1.21 (2)		0.998 (2)	12.883 (6)	0.541 (9)	30.81 (2)
	293.15	0.651	2.41 (3)		0.999 (1)	16.45 (1)	1.20 (1)	22.79 (2)
	393.15	0.124		1.42 †				
	393.15	0.143	1.749 (9)		0.921 (3)	9.176 (6)	0.568 (3)	31.58 (2)
	393.15	0.500	7.38 (4)		0.971 (1)	11.94 (3)	2.85 (2)	20.62 (4)
	393.15	0.750	13.13 (8)		0.960 (2)	14.2 (2)	6.85 (4)	10.39 (9)
Phosgene + Benzene								
	293.15	0.023	0.017 (1)	0.018[71]	0.44 (3)	11.248 (5)	0.0070 (4)	35.11 (2)
	293.15	0.069	0.029 (2)	0.031[71]	0.73 (2)	11.348 (5)	0.0120 (8)	34.50 (2)
	293.15	0.137	0.046 (2)	0.045[71]	0.85 (2)	11.499 (4)	0.0190 (8)	33.63 (2)
	293.15	0.198	0.061 (2)	0.056[71]	0.89 (1)	11.651 (7)	0.0250 (8)	32.88 (2)
	293.15	0.248	0.069 (3)	0.065[71]	0.88 (2)	11.777 (6)	0.029 (1)	32.30 (2)
	293.15	0.332	0.084 (3)	0.081[71]	0.923 (7)	11.973 (5)	0.035 (1)	31.26 (2)
	293.15	0.370	0.085 (3)	0.086[71]	0.935 (7)	12.060 (6)	0.036 (1)	30.80 (2)
	293.15	0.461	0.098 (4)	0.098[71]	0.942 (6)	12.300 (5)	0.041 (2)	29.79 (2)
	293.15	0.650	0.122 (4)		0.965 (5)	12.830 (6)	0.052 (2)	27.77 (2)
	293.15	0.800	0.133 (3)		0.980 (2)	13.294 (6)	0.056 (1)	26.36 (1)
Phosgene + Chlorobenzene								
	323.15	0.234	0.102 (4)	0.103 †	0.97 (1)	10.330 (5)	0.039 (2)	38.83 (3)
	323.15	0.600	0.254 (5)		0.99 (1)	11.641 (6)	0.099 (2)	31.33 (2)
	423.15	0.200	0.77 (1)		0.822 (6)	8.984 (5)	0.239 (3)	32.92 (2)
	423.15	0.431	1.47 (2)		0.918 (3)	9.451 (9)	0.485 (7)	27.77 (3)
	423.15	0.800	2.65 (3)		0.975 (1)	10.01 (1)	1.00 (1)	19.10 (3)
	448.15	0.200	1.08 (1)		0.760 (6)	8.63 (1)	0.324 (3)	31.07 (3)
	448.15	0.451	2.16 (2)		0.892 (2)	9.03 (1)	0.706 (7)	25.21 (4)
	448.15	0.800	3.86 (3)		0.959 (1)	9.20 (4)	1.54 (1)	16.04 (5)

Table 5. Continued

Mixture (A + B)	T (K)	x_A (mol/mol)	p (MPa)	p^{exp} (MPa)	y_A (mol/mol)	ρ' (mol/l)	ρ'' (mol/l)	Δh_v (kJ/mol)
Phosgene + Ortho-Dichlorobenzene								
	343.15	0.131	0.097 (8)		0.988 (9)	8.946 (5)	0.034 (3)	47.81 (3)
	343.15	0.401	0.32 (2)		0.998 (2)	9.965 (7)	0.119 (7)	39.74 (4)
	343.15	0.700	0.50 (2)		0.999 (1)	11.302 (9)	0.188 (8)	30.76 (3)
	363.15	0.080	0.105 (5)	0.103 †	0.97 (1)	8.611 (5)	0.035 (2)	47.96 (3)
	363.15	0.401	0.48 (1)		0.998 (2)	9.731 (4)	0.170 (2)	38.38 (2)
	363.15	0.700	0.81 (2)		0.999 (1)	10.958 (6)	0.301 (7)	29.30 (2)
Phosgene + Toluene								
	308.15	0.102	0.033 (2)	0.034 †	0.87 (1)	9.611 (5)	0.0129 (8)	39.10 (3)
	308.15	0.242	0.069 (3)		0.952 (5)	10.102 (5)	0.027 (1)	36.77 (2)
	308.15	0.700	0.190 (5)		0.9969 (7)	12.017 (6)	0.077 (2)	28.90 (2)
	423.15	0.200	0.81 (1)		0.698 (8)	8.433 (9)	0.258 (3)	29.60 (3)
	423.15	0.530	1.83 (2)		0.893 (3)	9.20 (1)	0.635 (7)	23.43 (3)
	423.15	0.750	2.48 (2)		0.948 (1)	9.62 (2)	0.926 (7)	19.11 (4)
	448.15	0.200	1.24 (2)		0.639 (8)	8.048 (9)	0.386 (6)	27.47 (4)
	448.15	0.426	2.12 (3)		0.812 (4)	8.46 (1)	0.71 (1)	23.15 (3)
	448.15	0.750	3.55 (5)		0.925 (1)	8.78 (4)	1.38 (2)	16.12 (6)

The number in parentheses indicates the statistical uncertainty in the last digit. The experimental data from this work is marked by †.

the simulation results for $\xi = 1$ strongly deviate from the experimental bubble points at the low temperature.

Hydrogen chloride + benzene

Figure 13 depicts the VLE of hydrogen chloride + benzene at 293.15 and 393.15 K. The bubble point vapor pressure supplied by BASF at ambient temperature (293.15 K) in the benzene-rich region ($x_{HCl} = 0.043$ mol/mol) was taken to adjust the binary parameter of the molecular model $\xi = 1.112$ and of the Peng-Robinson EOS $k_{ij} = -0.077$.

The simulation results are in very good agreement with the Peng-Robinson EOS for both temperatures; some deviations are present in the extended critical region at 393.15 K. The models consistently predict a concave bubble line. These data sets are supported by the experimental bubble point at 393.15 K, cf. Figure 13. Please note that this experimental bubble point was not considered in the fitting procedure, it was supplied after the calculations.

Hydrogen chloride + chlorobenzene

In Figure 14, the VLE of hydrogen chloride + chlorobenzene at 283.15, 393.15, and 423.15 K is presented. Here, the isotherm at 283.15 K is subcritical, for the other two temperatures hydrogen chloride is supercritical.

Both ξ and k_{ij} were adjusted in the chlorobenzene-rich composition range ($x_{HCl} = 0.094$ mol/mol) at 283.15 K, where one experimental bubble point was made available by BASF. The binary parameter of the molecular mixture model is $\xi = 1.020$ and the one of the Peng-Robinson EOS is zero. The simulation results and those from the Peng-Robinson EOS are consistent, except in the extended critical region of the mixture, where some deviations occur. Again, both models predict a concave bubble line at elevated temperatures. Furthermore, the dew line at 283.15 K indicates that the saturated vapor contains almost exclusively hydrogen chloride. The subsequently supplied experimental bubble point at 393.15 K, cf. Figure 14, supports again both models.

Hydrogen chloride + ortho-dichlorobenzene

The mixture hydrogen chloride + ortho-dichlorobenzene is a unique case in this study, as no experimental VLE data were available during the model development. Figure 15 shows the isotherm 393.15 K. Hydrogen chloride is supercritical at this temperature and the dew line is very close to pure hydrogen chloride. Without experimental data for adjustment, $\xi = 1$ and $k_{ij} = 0$ were adopted for the molecular model and the Peng-Robinson EOS, respectively. The results of the two models are generally in good agreement, however, with increasing deviations in the extended critical region. Again, both models predict a concave bubble line. The subsequently supplied experimental bubble point, cf. Figure 15, is in very good agreement, particularly with the simulation data.

Hydrogen chloride + toluene

Figure 16 shows the VLE of hydrogen chloride + toluene for 293.15 and 393.15 K. For this mixture, a single experimental bubble point at ambient temperature ($x_{HCl} = 0.048$ mol/mol) was made available by BASF for the adjustment of the binary parameters ($\xi = 0.981$ and $k_{ij} = -0.075$).

Simulation results and Peng-Robinson EOS show similar trends, significant deviations are present for the higher temperature, especially on the bubble line approaching the critical region. The bubble line is again concave, as for all mixtures containing hydrogen chloride studied in this work. Figure 16 presents one additional subsequently supplied bubble point at 393.15 K that supports the results of both models.

Phosgene + benzene

In Figure 17, another topology of the two-phase envelope can be seen for the mixture phosgene + benzene. At ambient temperature (293.15 K), phosgene + benzene has a binary vapor pressure which is close to ambient conditions, both components are subcritical and the bubble line is S-shaped.

The publicly available experimental data at this temperature by Kireev et al.[71] are ten bubble points in the benzene-

rich region. The binary parameters $\xi = 0.960$ and $k_{ij} = 0.05$ were adjusted at 293.15 K and $x_{\text{phosgene}} = 0.37$ mol/mol. Both the simulation results and the Peng-Robinson EOS match almost perfectly with the experimental data, but the phase envelope from simulation is a little wider than the one from the EOS.

Phosgene + chlorobenzene

The VLE of phosgene + chlorobenzene is presented in Figure 18 at 323.15, 423.15, and 448.15 K. Experimental data on the bubble line supplied by BASF at 323.15 K in the chlorobenzene-rich region ($x_{\text{phosgene}} = 0.234$ mol/mol) were taken for the optimization of the models, yielding $\xi = 0.990$ and $k_{ij} = 0.006$.

For this mixture, Peng-Robinson EOS and simulation results agree very well for all three temperatures on the bubble line and on the dew line. Both models predict a concave bubble line. Audette et al.[73] determined the bubble line at 448 K, cf. Figure 18. Considering the obvious scatter of that experimental data, the results of both models studied here are well supported.

Phosgene + ortho-dichlorobenzene

Figure 19 shows the wide VLE envelope of the mixture phosgene + ortho-dichlorobenzene at 343.15 and 363.15 K. The dew lines are very close to the low boiling pure substance (phosgene) in this case. One experimental bubble point at 363.15 K and $x_{\text{phosgene}} = 0.080$ mol/mol was made available by BASF for this mixture. No adjustment was necessary for the molecular model as the vapor pressure predicted with $\xi = 1.000$ matches the experimental number well. The adjustment of the binary parameter of the EOS yielded $k_{ij} = 0.02$.

A very good agreement between simulation results and Peng-Robinson EOS on both the bubble line and the dew line was found throughout. However, no additional experimental VLE data are available for this mixture for an assessment, but based on the results discussed above, it can be expected that the predictions for this mixture are reliable. The fact that the predictions from the EOS and those from molecular simulation, hence from two structurally different methods, agree well, gives additional confidence.

Phosgene + toluene

The VLE of phosgene + toluene is presented at 308.15, 423.15, and 448.15 K in Figure 20. One experimental bubble point was made available by BASF at 308.15 K in the toluene-rich region. The binary parameters $\xi = 0.990$ and $k_{ij} = 0.01$ were adjusted at this temperature and $x_{\text{phosgene}} = 0.102$ mol/mol. Here, throughout an almost perfect agreement between the simulation results and the Peng-Robinson EOS was found on the bubble line and on the dew line. As before, unfortunately no additional VLE data are available for a further assessment, but it can be expected that the results are reliable.

Conclusions

Molecular modeling and simulation was applied to predict VLE of binary mixtures containing hydrogen chloride and phosgene in combination with benzene, chlorobenzene, ortho-dichlorobenzene, and toluene. New molecular models were developed for these six components based on QC information on molecular geometry and electrostatics. Furthermore, experimental data on the vapor pressure and the saturated liquid density were taken into account to optimize the pure substance models. These pure substance properties were accurately described by the molecular models from the triple point to the critical point. Average deviations to correlations of experimental data are typically less than 5 and 0.5 % for vapor pressure and saturated liquid density, respectively. Critical values of temperature, density, and pressure from simulation agree with experimental data within the combined error bars.

The design of the models for the cyclic components allows for their compatibility with molecular hydrogen chloride models by distributing the quadrupolar interaction sites among the methine groups.

The second virial coefficient was predicted for hydrogen chloride, phosgene and benzene and favorably compared to experimental data. The other three substances were not studied with respect to this property as there are no data available for comparison.

For an optimized description of the binary VLE, the unlike dispersive interaction was adjusted for seven of the nine studied binary systems to a single experimental bubble point in the vicinity of ambient conditions. With these binary mixture models, VLE data, including dew point composition, saturated densities, and enthalpy of vaporization, were predicted for a wide range of temperatures and compositions. The predictions show a good agreement with additional experimental binary VLE data that were not considered in the model development.

This work shows that molecular modeling and simulation can successfully be used to predict thermophyiscal data of industrially important pure substances and mixtures. It was applied here to properties that can also be described well by phenomenological approaches like EOS. Nevertheless, even in such cases, molecular modeling and simulation is valuable as it provides and independent approach where no experimental data are available.

Acknowledgments

The authors acknowledge Deutsche Forschungsgemeinschaft for funding this project. The presented research was conducted under the auspices of the Boltzmann-Zuse Society of Computational Molecular Engineering (BZS), and the simulations were performed on the national super computer NEC SX-8 at the High Performance Computing Center Stuttgart (HLRS) and on the HP X6000 super computer at the Steinbuch Centre for Computing, Karlsruhe. The authors would like to thank Xijun Fu, Tianmin Du, and Shan Yuan for handling numerous simulation runs and helping to prepare the material for publication.

Literature Cited

1. Maginn EJ. From discovery to data: what must happen for molecular simulation to become a mainstream chemical engineering tool. *AIChE J*. 2009;55:1304–1310.
2. Case F, Chaka A, Friend DG, Frurip D, Golab J, Johnson R, Moore J, Mountain RD, Olson J, Schiller M, Storer J. The first industrial fluid properties simulation challenge. *Fluid Phase Equilib*. 2004; 217:1–10.

3. Case F, Chaka A, Friend DG, Frurip D, Golab J, Gordon P, Johnson R, Kolar P, Moore J, Mountain RD, Olson J, Ross R, Schiller M. The second industrial fluid properties simulation challenge. *Fluid Phase Equilib.* 2005;236:1–14.
4. Case FH, Brennan J, Chaka A, Dobbs KD, Friend DG, Frurip D, Gordon PA, Moore J, Mountain RD, Olson J, Ross RB, Schiller M, Shen VK. The third industrial fluid properties simulation challenge. *Fluid Phase Equilib.* 2007;260:153–163.
5. Case FH, Brennan J, Chaka A, Dobbs KD, Friend DG, Gordon PA, Moore JD, Mountain RD, Olson JD, Ross RB, Schiller M, Shen VK, Stahlberg EA. The fourth industrial properties simulation challenge. *Fluid Phase Equilib.* 2008;274:2–9.
6. Case FH, Chaka A, Moore JD, Mountain RD, Olson JD, Ross RB, Schiller M, Shen VK, Stahlberg EA. The fifth industrial fluid properties simulation challenge. *Fluid Phase Equilib.* 2009;285:1–3.
7. Vrabec J, Stoll J, Hasse H. Molecular models of unlike interactions in fluid mixtures. *Mol Sim.* 2005;31:215–221.
8. www.ms-2.de
9. Jones JE. On the determination of molecular fields. I. From the variation of the viscosity of a gas with temperature. *Proc Roy Soc.* 1924;106A:441–462.
10. Jones JE. On the determination of molecular fields. II. From the equation of state of a gas. *Proc Roy Soc.* 1924;106A:463–477.
11. Allen MP, Tildesley DJ. *Computer Simulations of Liquids*. Oxford: Oxford University Press, 1987.
12. Gray CG, Gubbins KE. *Theory of Molecular Fluids. 1. Fundamentals*. Oxford: Clarendon Press, 1984.
13. Lorentz HA. Über die anwendung des satzes vom virial in der kinetischen theorie der Gase. *Ann d Phys.* 1881;12:127–136.
14. Berthelot D. Sur le mélange des gaz. *Comput Rend Ac Sc.* 1898; 126:1703–1706.
15. Sandler SI, Castier M. Computational quantum mechanics: an underutilized tool in thermodynamics. *Pure Appl Chem.* 2007;79:1345–1359.
16. Schmidt MW, Baldridge KK, Boatz JA, Elbert ST, Gordon MS, Jensen JH, Koseki S, Matsunaga N, Nguyen KA, Shujun S, Windus TL, Dupuis M, Montgomery AM. General atomic and molecular electronic structure system. *J Comput Chem.* 1993;14:1347–1363.
17. Ungerer P, Beauvais C, Delhommelle J, Boutin A, Rousseau B, Fuchs AH. Optimization of the anisotropic united atoms intermolecular potential for n-alkanes. *J Chem Phys.* 2000;112:5499–5510.
18. Eggenberger R, Gerber S, Huber H, Welker M. A new ab initio potential for the neon dimer and its application in molecular dynamics simulations of the condensed phase. *Mol Phys.* 1994;82:689–699.
19. Vogt PS, Liapine R, Kirchner B, Dyson AJ, Huber H, Marcelli G, Sadus RJ. Molecular simulation of the vapour-liquid phase coexistence of neon and argon using ab initio potentials. *Phys Chem Chem Phys.* 2001;3:1297–1302.
20. Garrison SL, Sandler SI. On the use of ab initio interaction energies for the accurate calculation of thermodynamic properties. *J Chem Phys.* 2002;117:10571–10580.
21. Nasrabad AE, Laghaei R, Deiters UK. Prediction of the thermophysical properties of pure neon, pure argon, and the binary mixtures neon-argon and argon-krypton by Monte Carlo simulation using ab initio potentials. *J Chem Phys.* 2004;121:6423–6434.
22. Ermakova E, Solca J, Huber H, Welker M. Argon in condensed phase: quantitative calculations of structural, thermodynamic, and transport properties from pure theory. *J Chem Phys.* 1995;102:4942–4951.
23. Nasrabad AE, Deiters UK. Prediction of thermodynamic properties of krypton by Monte Carlo simulation using ab initio interaction potentials. *J Chem Phys.* 2003;119:947–952.
24. Leonhard K, Deiters UK. Monte Carlo simulations of nitrogen using an ab initio potential. *Mol Phys.* 2002;100:2571–2585.
25. Welker M, Steinebrunner G, Solca J, Huber H. Ab initio calculation of the intermolecular potential energy surface of $(CO_2)_2$ and first applications in simulations of fluid CO_2. *Chem Phys.* 1996;213:253–261.
26. Naicker PK, Sum AK, Sandler SI. Ab initio pair potential and phase equilibria predictions for Hydrogen chloride. *J Chem Phys.* 2003; 118:4086–4093.
27. Hloucha M, Sum AK, Sandler SI. Computer simulation of acetonitrile and methanol with ab initio-based pair potentials. *J Chem Phys.* 2000;113:5401–5406.
28. Garrison SL, Sandler SI. An accurate acetylene intermolecular potential for phase behavior predictions from quantum chemistry. *J Phys Chem.* 2004;108:18972–18979.
29. Garrison SL, Sandler SI. A potential from quantum chemistry for thermodynamic property predictions for methanethiol. *J Chem Phys.* 2005;123:054506.
30. Stoll J. *Molecular Models for the Prediction of Thermalphysical Properties of Pure Fluids and Mixtures. Fortschritt-Berichte VDI, Reihe 3, Vol. 836*. Düsseldorf: VDI-Verlag, 2005.
31. Eckl B, Vrabec J, Hasse H. Set of molecular models based on quantum mechanical ab initio calculations and thermodynamic data. *J Phys Chem B.* 2008;112:12710–12721.
32. Bourasseau E, Haboudou M, Boutin A, Fuchs AH, Ungerer P. New optimization method for intermolecular potentials: optimization of a new anisotropic united atoms potential for olefins: prediction of equilibrium properties. *J Chem Phys.* 2003;118:3020–3034.
33. Rowley RL, Wilding WV, Oscarson JL, Yang Y, Zundel NA, Daubert TE, Danner RP. *DIPPR® Data Compilation of Pure Compound Properties. Design Institute for Physical Properties*. New York: AIChE, 2006.
34. Lotfi A, Vrabec J, Fischer J. Vapour liquid equilibria of the Lennard-Jones fluid from the NpT plus test particle method. *Mol Phys.* 1992;76:1319–1333.
35. Vrabec J, Hasse H. Grand equilibrium: vapour-liquid equilibria by a new molecular simulation method. *Mol Phys.* 2002;100:3375–3383.
36. Mathews JF. The critical constants of inorganic substances. *Chem Rev.* 1972;72:71–100.
37. Ambrose D. Vapor–liquid critical properties. National Physical Laboratory Report Chem 107, Middlesex, United Kingdom, 1980.
38. Ambrose D, Tsonopoulos C. Vapor–liquid critical properties of elements and compounds. III. Aromatic hydrocarbons. *J Chem Eng Data.* 1995;40:547–558.
39. Alani GH, Kudchadker AP, Zwolinski BJ. The critical constants of organic substances. *Chem Rev.* 1968;68:659–735.
40. Bunger WB, Riddick JA. *Organic Solvents: Physical Properties and Methods of Purification*, *3rd ed.* New York: Wiley Online Library, 1970.
41. Danner RP, Tarakad RR. An improved corresponding states method for polar fluids: correlation of second virial coefficients. *AIChE J.* 1977;23:685–695.
42. Nunes Da Ponte M, Staveley LAK. The equation of state and thermodynamic properties of liquid hydrogen chloride. *J Chem Thermodyn.* 1981;13:179–186.
43. Tsonopoulos C. Second virial coefficients of water pollutants. *AIChE J.* 1978;24:1112–1115.
44. Polt A, Platzer B, Maurer G. Parameter der thermischen Zustandsgleichung von Bender für 14 mehratomige reine Stoffe. *Chem Tech (Leipzig).* 1992;44:216–224.
45. De Leiuw FH, Dymanus A. Magnetic properties and molecular quadrupole moment of HF and HCl by molecular-beam electric-resonance spectroscopy. *J Mol Spectrosc.* 1973;48:427–445.
46. Buth C, Paulus B. Hydrogen bonding in infinite hydrogen fluoride and hydrogen chloride chains. *Phys Rev B.* 2006;74:0450122.
47. Meredith AW, Liu M, Nordholm S. Quantum chemical exploration of the HC1 dimer interaction. *Chem Phys.* 1997;220:63–68.
48. Horvath AL. *Physical Properties of Inorganic Compounds*. New York: Crane Russak, 1975.
49. Howe JA, Flygare WH. Strong field stark effect. *J Chem Phys.* 1961;36:650–652.
50. Wu L, Yang QY, Zhong CL. Molecular simulation of vapor–liquid equilibria of toxic gases. *Fluid Phase Equilib.* 2004;220:1–6.
51. Stull DR. *Thermodynamic Functions of Gases*. London: Butterworth Scientific Publications, 1956.
52. Bonnaud P, Nieto-Draghi C, Ungerer P. Anisotropic united atom model including the electrostatic interactions of benzene. *J Phys Chem B.* 2007;111:3730–3741.
53. Carrero-Mantilla J. Simulation of the (vapor + liquid) equilibria of binary mixtures of benzene, cyclohexane, and hydrogen. *J Chem Thermodyn.* 2008;40:271–283.
54. Errington JR, Panagiotopoulos AZ. New intermolecular potential models for benzene and cyclohexane. *J Chem Phys.* 1999;111:9731–9738.
55. Contreras-Camacho RO, Ungerer P, Boutin A, Mackie AD. Optimized intermolecular potential for aromatic hydrocarbons based on anisotropic united atoms. 1. Benzene. *J Phys Chem B.* 2004;108: 14109–14114.

56. Wick CD, Martin MG, Siepmann JI. Transferable potentials for phase equilibria. 4. United-atom description of linear and branched alkenes and alkylbenzenes. *J Phys Chem B*. 2000;104:8008–8016.
57. Smith BD. *Thermodynamic Data for Pure Compounds. Part A. Hydrocarbons and Ketones*. Amsterdam: Elsevier, 1986.
58. American Petroleum Institute Research Project 44. Selected values of properties of hydrocarbons and related compounds. Thermodynamic Research Center, Texas A&M University, College Station, Texas, 1980.
59. Poynter RL. Microvawe spectrum, quadrpolar constants, and dipole moment of chlorobenzene. *J Chem Phys*. 1963;39:1962–1966.
60. Othmer DF. *Concise Encyclopedia of Chemical Technology*, 5th ed. New York: Wiley, 2007.
61. Srivastava R, Smith BD. Total pressure vapor—liquid equilibrium data for binary systems of dichloromethane with benzene, toluene, nitromethane, and chlorobenzene. *J Chem Eng Data*. 1985;30:313–318.
62. Hurdis EC, Smyth CP. Dipole moments in the vapor state and resonance effects in some substituted benzenes. *J Am Chem Soc*. 1942; 64:2212–2216.
63. Hu J, White D, Johnston HL. Condensed gas calorimetry. V. heat capacities, latent heats and entropies of fluorine from 13 to 85 K; heats of transition, fusion, vaporization and vapor pressures of the liquid. *J Am Chem Soc*. 1953;75:5642–5645.
64. Kreiner WA, Rudolph HD, Tan BT. Microwave spectra of several molecular isotopes of toluene. *J Mol Sectreosc*. 1973;48:86–99.
65. Nieto-Draghi C, Bonnaud P, Ungerer P. Anisotropic united atom model including the electrostatic interactions of methylbenzenes. I. Thermodynamic and structural properties. *J Phys Chem C*. 2007; 111:15686–15699.
66. Contreras-Camacho RO, Ungerer P, Ahunbay MG, Lachet V, Perez-Pellitero J, Mackie AD. Optimized intermolecular potential for aromatic hydrocarbons based on anisotropic united atoms. 2. Alkylbenzenes and styrene. *J Phys Chem B*. 2004;108:14115–14123.
67. Schnabel T, Vrabec J, Hasse H. Unlike Lennard-Jones parameters for vapor–liquid equilibria. *J Mol Liq*. 2007;135:170–178.
68. Carrero-Mantilla J, Llano-Restrepo M. Further validation of a set of quadrupolar potential models for ethylene and propylene from the prediction of some binary mixture vapor–liquid equilibria by Gibbs-ensemble molecular simulation. *Mol Sim*. 2003;29:549–554.
69. Stoll J, Vrabec J, Hasse H. Vapor–liquid equilibria of mixtures containing nitrogen, oxygen, carbon dioxide, and ethane. *AIChE J*. 2003;49:2187–2198.
70. Gillespie PC, Cunningham JR, Wilson GM. Total pressure vapor–liquid equilibrium measurements for the Hydrogen chloride/vinyl chloride and Hydrogen chloride/phosgene systems. *AIChE Symp Ser*. 1985;81:49–56.
71. Kireev VA, Kaplan SI, Vasneva KI. Across the equilibrium of liquid mixtures and solutions: II. Phosgene vapor solubility in some solvents at pressures below atmospheric. *Zh Obshch Khim*. 1936;6: 799–805.
72. Peng DY, Robinson DB. A new two-constant equation of state. *Ind Eng Chem Fundam*. 1976;15:59–64.
73. Audette DE, Giordano DE, Wedlich RC. Estimating VLE of binary liquid solutions by ARC and GC. *J Therm Anal*. 1997;49:671–677.
74. Andersen HC. Molecular dynamics simulations at constant pressure and/or temperature. *J Chem Phys*. 1980;72:2384–2393.
75. Widom B. Some Topics in the theory of fluids. *J Chem Phys*. 1963; 39:2808–2812.
76. Nezbeda I, Kolafa J. A new version of the insertion particle method for determining the chemical potential by Monte Carlo simulation. *Mol Sim*. 1991;5:391–403.
77. Vrabec J, Kettler M, Hasse H. Chemical potential of quadrupolar two-centre Lennard-Jones fluids by gradual insertion. *Chem Phys Lett*. 2002;356:431–436.
78. Lustig R. Angle-average for the powers of the distance between two separated vectors. *Mol Phys*. 1988;65:175–179.
79. Flyvbjerg H, Petersen HG. Error estimates on averages of correlated data. *J Chem Phys*. 1989;91:461–466.

Appendix

The Grand Equilibrium method[35] was used to calculate VLE data. For the liquid, molecular dynamics simulations were performed in the isobaric-isothermal (*NpT*) ensemble using isokinetic velocity scaling[11] and Anderson's barostat.[74] There, the number of molecules was 864 throughout and the time step was 1 to 3 fs depending on the molecular weight and the magnitude of the intermolecular interactions. The initial configuration was a face centered cubic lattice; the fluid was equilibrated over 25,000 time steps with the first 5,000 time steps in the canonical (*NVT*) ensemble. The production run time span was 200,000 to 300,000 time steps with a membrane mass of 10^9 kg/m^4. Widom's insertion method[75] was used to calculate the chemical potential of hydrogen chloride as a pure substance and in the mixture with phosgene by inserting 3,456 test molecules every production time step.

In all other cases Widom's insertion method yielded large statistical uncertainties for the chemical potential in the liquid, which is due to the high densities and the strongly interacting molecules. Instead, Monte Carlo simulations were performed in the *NpT* ensemble for the liquid. Thereby, the chemical potential was calculated by the gradual insertion method.[76,77] The number of molecules was 500. Starting from a face centered cubic lattice, 15,000 Monte Carlo cycles were performed for equilibration and 50,000 for production, each cycle containing 500 translation moves, 500 rotation moves, and 1 volume move. Every 50 cycles, 5000 fluctuating state change moves, 5000 fluctuating particle translation/rotation moves, and 25,000 biased particle translation/rotation moves were performed, to determine the chemical potential. These computationally demanding simulations yield the chemical potential in dense and strong interacting liquids with high accuracy, leading to reasonable uncertainties in the VLE.

For the corresponding vapor, Monte Carlo simulations in the pseudo-μVT ensemble were performed. The simulation volume was adjusted to lead to an average number of 500 molecules in the vapor phase. After 2000 initial *NVT* Monte Carlo cycles, starting from a face centered cubic lattice, 10,000 equilibration cycles in the pseudo-μVT ensemble were performed. The length of the production run was 50,000 cycles. One cycle is defined here to be a number of attempts to displace and rotate molecules equal to the actual number of molecules plus three insertion and three deletion attempts.

The cut-off radius was set to 17.5 Å throughout and a center of mass cut-off scheme was used. LJ long-range interactions beyond the cut-off radius were corrected using angle averaging as proposed by Lustig.[78] Electrostatic interactions were approximated by a resulting molecular dipole and corrected using the reaction field method.[11] Statistical uncertainties of the simulated values were estimated by a block averaging method.[79]

Manuscript received Feb. 14, 2010, and revision received May 8, 2010.